A 20-million-year Early Jurassic cyclostratigraphic record and its implications for the chaotic inner Solar System and sea-level changes

Guillaume Charbonnier, Slah Boulila, Bruno Galbrun, Jacques Laskar, Silvia Gardin, Isabelle Rouget

Charbonnier G., Boulila S., Galbrun B., Laskar J., Gardin S., Rouget I. (2023). A 20-million-year Early Jurassic cyclostratigraphic record and its implications for the chaotic inner Solar System and sea-level changes. *Basin Research*, https://doi.org/10.1111/bre.12754

A 20-million-year Early Jurassic cyclostratigraphic record and its implications for the chaotic inner Solar System and sea-level changes

Guillaume Charbonnier[1*], Slah Boulila[1,2], Bruno Galbrun[1], Jacques Laskar[2], Silvia Gardin[3], Isabelle Rouget[3]

[1]Sorbonne Universités, CNRS, ISTeP (Institut des Sciences de la Terre-Paris), F-75005 Paris, France.
[2]ASD, IMCCE-CNRS UMR 8028, Observatoire de Paris, PSL Research University, Sorbonne Université, 77 avenue Denfert-Rochereau, 75014 Paris, France.
[3]Sorbonne Universités, MNHN, CNRS, CR2P (Centre de Recherche en Paléontologie–Paris), F-75005 Paris, France.

* Corresponding author.
E-mail address: guillaume.charbonnier@sorbonne-universite.fr (G. Charbonnier)

Abstract

We present high-resolution (every 2 cm) magnetic susceptibility (MS) data from the Sancerre-Couy drill-core (Paris Basin), spanning the latest Sinemurian to the earliest Aalenian (early Jurassic). This record allows to build a 20-million-year cyclostratigraphic interval using the stable 405 kyr (g2–g5) orbital eccentricity cycle and to focus on long-period cyclicities and their potential implications for the chaotic diffusion in the inner Solar System and sea level changes. Time series analysis indicates evidence of two long-period cyclicities of 1.6 and 3.4 Myr. These Early Jurassic cyclicities likely correspond to the Cenozoic orbital cyclicities of 2.4 Myr (g4–g3) and 4.7 Myr eccentricity terms. Shortening of eccentricity terms during the Early Jurassic is potentially related to the chaotic orbital motion of the inner planets expressed in the resonant argument $\theta = 2(g4 - g3) - (s4 - s3)$. The 1.6 Myr (g4–g3) cycle matches the third-order eustatic sequences, while the 3.4 Myr cycle has no equivalent in the reference eustatic chart. To these cycles of several million years are superimposed a cyclicity of ~7.5 Myr, which may correspond to the eccentricity term of 9.5 Myr, previously detected in the Cenozoic. Such cyclicity matches the global, "shorter" second order sea level sequences, and is strongly documented in the sedimentological and mineralogical proxy data, hence supporting the potential key role of orbitally paced climate and sea-level changes at this timescale.

Key words: Early Jurassic, cyclostratigraphy, Paris Basin, astronomical implications, sea level.

1. Introduction

The cyclic variations of the Earth's orbit and its spin axis (precession, obliquity, eccentricity) due to gravitational interactions with the other planets modulate seasonal insolation and drive climate changes on the Earth's surface (e.g., Milankovitch, 1941; Hays et al., 1976). Long-period (Myr to multi-Myr) astronomical (Milankovitch) cycles, which manifest as amplitude modulation (AM) of the eccentricity and obliquity cycles, may have a significant impact on global climate, sea-level and biogeochemical variations, (e.g., Zachos et al., 2001; Pälike et al., 2006; Boulila et al., 2011, 2012; Sprovieri et al., 2013; Boulila, 2019, among many others).

The well-known Myr-scale Milankovitch cycles are the 1.2 Myr AM obliquity (s4–s3) and 2.4 Myr eccentricity (g4–g3) terms, where g3, g4 are related to the precession of the perihelions of the Earth and Mars, and s3, s4 are related to the precession of the nodes of the same planets (Laskar, 1990). These two cyclicities have been shown to strongly affect long-term climate and sea-level variations during icehouse and greenhouse periods (e.g., Pälike et al., 2006; Boulila et al., 2011). Additionally, the detection of 1.2 and 2.4 Myr orbital cycles in deep (pre-Cenozoic) geological times can provide valuable information for the chaotic behavior of planetary motions in the inner Solar System (Laskar et al., 2004) since the important resonant term $\theta = 2(g4 - g3) - (s4 - s3)$ includes these two periodicities (Laskar, 1990). Another long-period ~4.7 Myr orbital cyclicity has been less detected in the geological archives (Boulila et al., 2012, 2014, 2020; Boulila, 2019), which is probably related to the same resonant argument θ and corresponds to the libration frequency of θ (Laskar, 1990). Due to the chaotic behavior of the orbital motions of the Earth and Mars, the above related periods can evolve in time and reach very different values (e.g., Laskar, 1990; Laskar et al., 2004; Olsen et al., 2019). Mapping these periodicities in the sedimentary record, especially in pre-Cenozoic strata, can provide constraints on astronomical modeling (Laskar et al., 2004, 2011; Hinnov, 2013). A respectful number of cyclostratigraphic studies have focused on the expression of g4–g3 eccentricity period, especially in the Mesozoic strata, and provided promising results (Boulila et al., 2010, 2014; Huang et al., 2010a; Ikeda et al., 2010; Olsen et al., 2019; Mau et al., 2022). All of these studies detected a shortened g4–g3 eccentricity period (< 2.4 Myr), possibly in relation with the chaotic diffusion in the inner Solar System (Laskar, 1990).

The assessment of such multi-Myr Milankovitch periodicities requires the acquisition of very long (ten to tens of Myr) cyclostratigraphic time series. Here, we investigate a long, early Jurassic cyclostratigraphic record from the Sancerre drill-core in the Paris Basin, which spans the latest Sinemurian through the earliest Aalenian (almost 20 Myr long, according to Gradstein et al., 2020). We acquired high-resolution (each 2 cm) magnetic susceptibility (MS) data of latest Sinemurian through the latest Pliensbachian time interval, combined with pre-existing high-resolution (4 cm) MS data of latest Pliensbachian through the earliest Aalenian from the same core (Boulila et al., 2014) to build a ~20 Myr long MS cyclostratigraphic record. We have also integrated pre-existing (Boulila et al., 2014) and new ammonite and calcareous nannofossil data to provide a constrained biostratigraphic framework, useful for potential correlations with neighboring basins, such as the English Mochras site (Ruhl et al., 2016; Storm et al., 2020).

We have first assessed the chronology of the recovered late Jurassic time interval using the stable 405 kyr eccentricity (g2–g5) cyclicity (g2, g5 are related to the precession of the perihelions of Venus and Jupiter) for orbital tuning (Laskar et al., 2004), and compare it with previous cyclostratigraphic studies (Ruhl et al., 2016; Storm et al., 2020; Pieńkowski et al., 2021). Then, we focused on long-period (Myr to multi-Myr) cyclicities, and their potential implications for the chaotic diffusion in the inner Solar System. Finally, we discussed the

significance of the recovered long-period MS cyclicities in terms of sea-level changes (Haq et al., 1987; Hardenbol et al., 1998; Boulila et al., 2014).

2. Geological setting and stratigraphic framework

2.1. Geological setting

The Paris Basin is a low-subsidence Meso-Cenozoic intracratonic sedimentary basin (Bassoulet et al., 1993). During the Early Jurassic, the Paris Basin, was situated at a palaeolatitude of about ~30°N in a sub-basin of the North-European epicontinental seaway of the Peritethyan Realm (Fig. 1). The lower Jurassic sediments, deposited in an open-marine setting, consists mainly of marls and clays with variable proportions of carbonate. Terrigenous materials in the marine setting likely originated from weathering of emerged landmasses, the Central Massif in the south, the Armorican Massif in the west, the Rhenish Massif in the northeast, and the London-Brabant Massif in the north (Fig. 1).

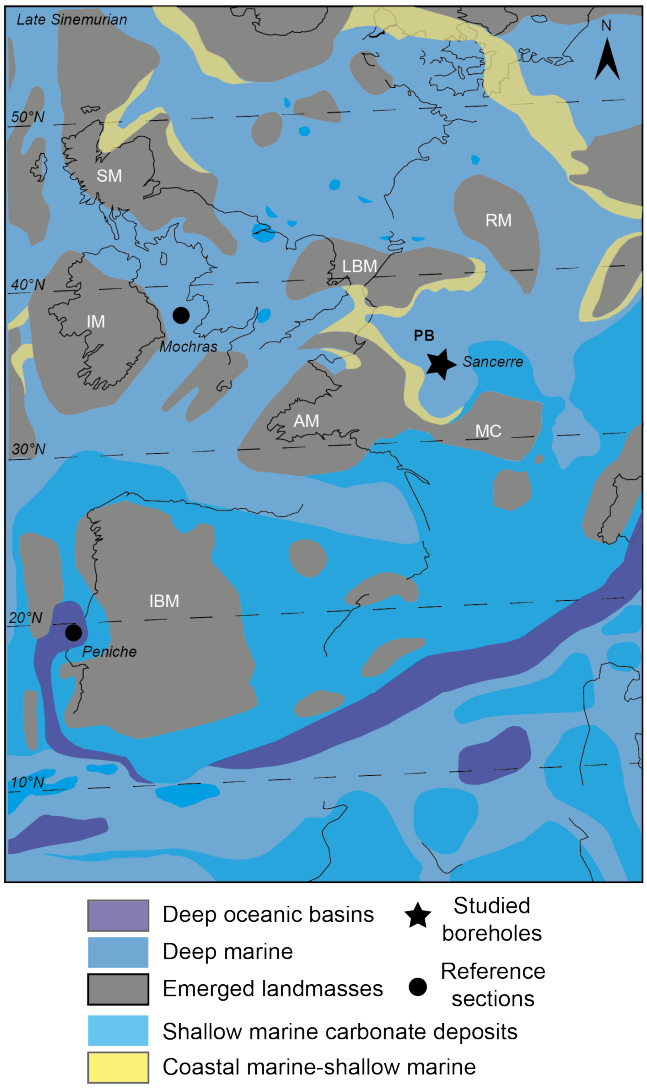

Fig. 1: Late Sinemurian paleogeography of Western Europe (modified from Thierry et al., 2000). IM: Iberian Massif; AM: Armorican Massif; MC: Massif Central; LBM: London-Brabant Massif; RM: Rhenish Massif; IM: Irish Massif; SM: Scotish Massif.

2.2. The Sancerre-Couy drill-core

The Sancerre-Couy-1 core, which provides a continuous recovery from the Callovian to the Carboniferous strata, is situated in the southwestern part of the Paris Basin (region of the "Cher"), 248 km south of Paris (40°1¢10. 8²N, 2°47¢6²E). It was drilled in 1986-1987 by the French « *Bureau de Recherches Géologiques et Minières* » (program GPF "*Géologie Profonde de la France*"; Lorenz et al., 1987). The uppermost Sinemurian-lowermost Aalenian interval in the Sancerre core is 245.45-m thick (194.55 to 440 m depth) (Fig. 2). The lithology of the uppermost Sinemurian-lower Pliensbachian interval consists of pale grey micritic limestone with *Gryphaea* alternating with dark-grey marls. The sedimentary succession from the upper part of the Pliensbachian (*Davoei-Spinatum* ammonites Zones) to the Toarcian becomes more marly with dark-grey marls and some carbonate-rich and silty light-grey marls. The initial age model of the core is based on a detailed biozonation by ammonites, bivalves, and calcareous nannofossils (Lorenz et al., 1987, 1991; Gély and Lorenz, 1991; Boulila et al., 2014; Peti et al., 2017) (Fig. 2), in addition to high-resolution carbon-isotope ($\delta^{13}C_{org}$) stratigraphy (Hermoso et al., 2009, 2012; Peti et al., 2017, 2021).

3. Material and methods

3.1. Biostratigraphy

3.1.1. Ammonites

An ammonite biozonation of the core was originally established by Lorenz et al. (1987, 1991). Recently, reinterpretation of the ammonite biozonation of the Sinemurian-lowermost Toarcian (from 450 to 340 m depth) and uppermost Pliensbachian-lowermost Aalenian (from 360 to 190 m depth) intervals was established by Peti et al. (2017) and Boulila et al. (2014), respectively. For this work a reconsideration of the previous determination of ammonites was made along the upper Pliensbachian interval *p.p.* (from 429 to 355.8 m depth; Table 1) (Fig. 3). The specimens were identified according to the systematic nomenclature for the Lower Jurassic ammonites.

3.1.2. Calcareous nannofossils

Previous calcareous nannofossil biostratigraphic frameworks has been established for the sequence from the uppermost Hettangian-lowermost Toarcian (from 513 to 340 m depth; Peti et al., 2017), and from the uppermost Pliensbachian-lowermost Aalenian (from 350 to 210 m depth; Boulila et al., 2014).

In this work we focused on the upper Pliensbachian *p.p.* interval, roughly corresponding to the *Stokesi-Solare* ammonite Sub-zones. A total of 126 new samples, 50 cm spaced, were collected from 410 to 355.8 m depth (Table 1) and processed as simple smear slides following standard technique (Fig. 4). For the biostratigraphic study, calcareous nannofossils were analyzed using a Zeiss Imaging II light microscope with a magnification of 1500. Three traverses corresponding to 450 fields of view per sample were examined to look for key nannofossil species, richness and abundance. The preservation of calcareous nannofossils has been evaluated using the SEM analysis as well as the visual criteria of Roth and Thierstein (1972) and Roth (1984). First and last occurrences of index species were used to establish a robust nannofossil biostratigraphic framework which ties with and completes that of Boulila et al, (2014) performed by the same team.

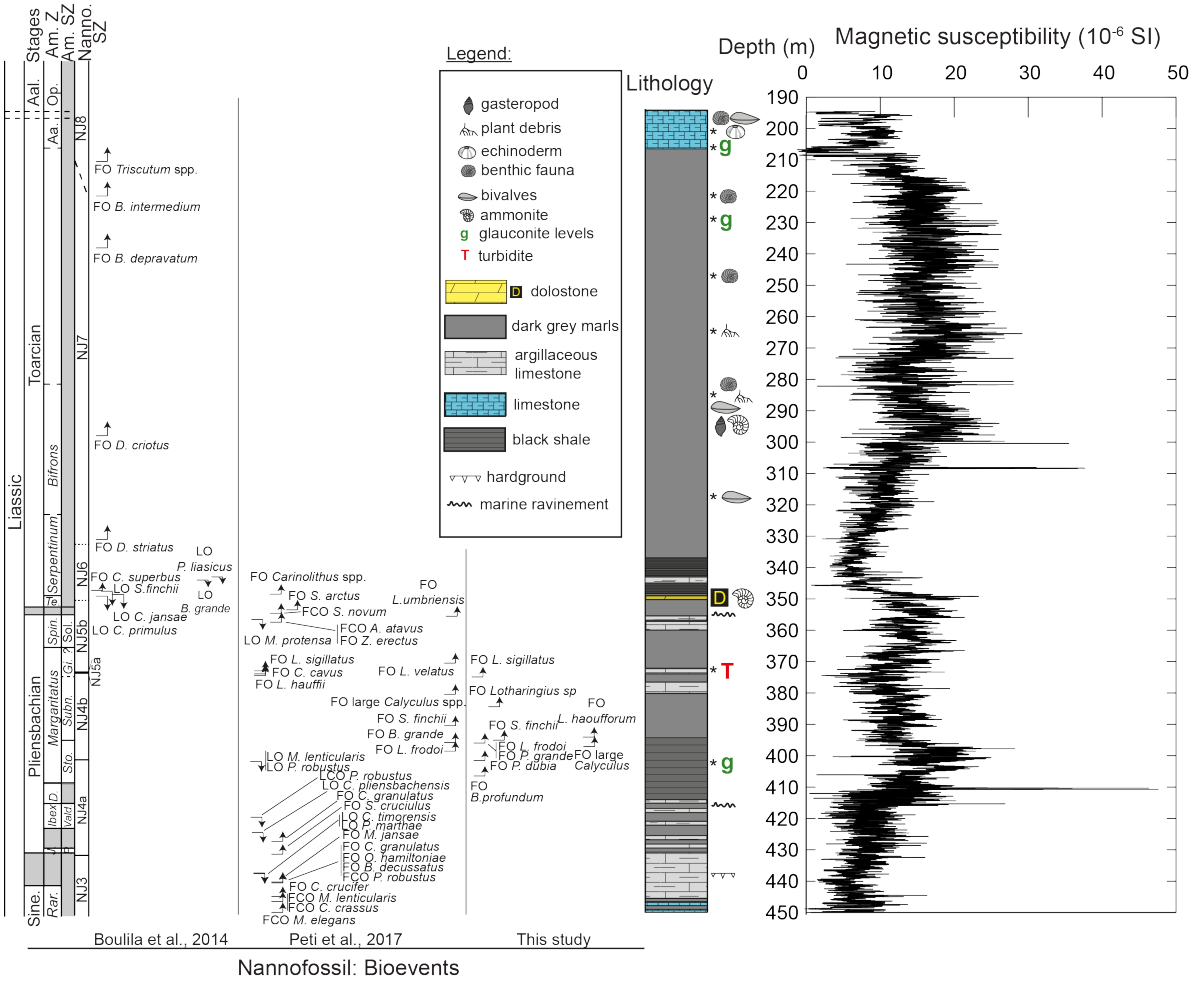

Fig. 2: Integrated stratigraphy, biostratigraphy, lithology, and magnetic susceptibility variations of the uppermost Sinemurian-lowermost Aalenian of the Sancerre core (Paris Basin). The stratigraphic framework is based on ammonites (Lorenz et al., 1987, 1991; Boulila et al., 2014; Peti et al., 2017; This work), and calcareous nannofossils (Boulila et al., 2014; Peti et al., 2017; This work). Depth scale is in meters below surface. Am. Z= Ammonite Zones; Am. SB= Ammonite Sub-Zones; Nanno. SZ= Nannofossil Sub-Zone. Rar.= Raricostatum ; J.= Jamesoni; D.= Davoei; Spin.= Spinatum; Te.= Tenuicostatum; Aa.= Aalensis; Op.= Opalinum; P.= Polymorphus; Vald.= Valdari; Subn.= Subnodosus; Gi.= Gibbosus; Sol.= Solare.

Fig. 3: Selected ammonites from the upper Pliensbachian interval: 1–3, *Pleuroceras* cf. *solare* (1) at 355.8 m; (2) at 364.15 m; (3) at 366.25 m. 4 and 6, *Amaltheus* cf *margaritatus*, (4) at 371.95 m; (6) at 386.9 m. (5), *Amaltheus cf. subnodosus* (at 374.98 m). 7 and 8, *Amaltheus stokesi* (at 406.5 m). 9, *Beicheiceras* indet (at 409.75 m). 10, *Aegoceras cf.capricornus* (at 410.75 m). 11, *Prodactylioceras davoei* (at 410 m). 12, *Aegoceras* or *Oistoceras* (at 414.53 m).

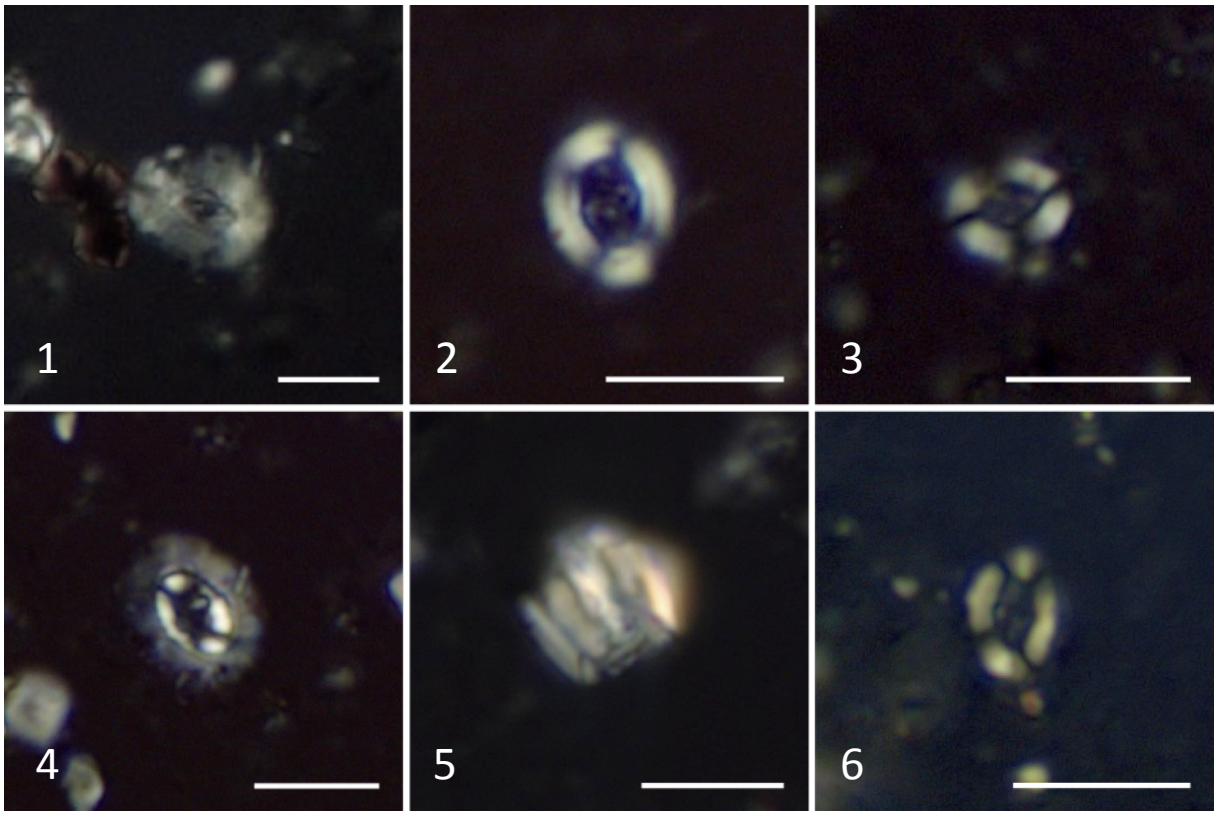

Fig. 4: Optical micrographs of main calcareous nannofossils bio-horizons, polarized light. Scale bar corresponds to 5µm. 1- *Biscutum finchii* (sample 389.7 m). 2- *Lotharingius sigillatus* (>5µ, sample 366.3 m). 3- *Lotharingiius sigillatus* (<5µ, sample 371.95 m). 4- *Biscutum grande* (sample 397 m). 5- *Parhabdolithus robustus* (sample 406.5 m). 6- *Lotharingius primitivus* (sample 403 m).

Table 1

Depth (m)	Stage	Taxon Ammonite	Ammonite Zone	Ammonite Sub-zone	Nannofossils bio-horizons (This work)
366.25	Upper Pliensbachian	*Pleuroceras apyrenum? or Solare ?*	Spinatum	Apyrenum	B *Lotharingius sigillatus* >5µm
371.95	Upper Pliensbachian	*Amaltheus margaritatus*	?		C *Lotharingius sigillatus* <5µm
372.15	Upper Pliensbachian	Bivalve			B *Lotharingius gr hauffi* (subcircular)
384.5					B *Lotharingius sigillatus* <5µm
389					T *Parhabdolithus robustus*
395	Upper Pliensbachian		*Margaritatus*		B *Similiscutum finchii*
396					B *Biscutum* grande
397	Upper Pliensbachian		*Margaritatus*		B large *Calyculus* spp
401.5	Upper Pliensbachian	*Amaltheus+ protogrammoceras? /Fuciniceras?*	*Margaritatus*	*Subnodosus*	B *Biscutum dubium*
403					B *Lotharingius* cf *L. primitivus*
406.5	Upper Pliensbachian	*Amaltheus stokesi*	*Margaritatus*	*Stokesi*	B *B.* cf *B. profundum*
409.5	Lower Pliensbachian	*Aegoceras*	*Davoei*		*Bussonius* spp; *L. barozi*, *C. granulatus* *C. jansae*; *Calyculus* flat, *A. atavus* *S. cruciulus* already present

Table 1: Reliability of calcareous nannofossils bio-horizons recorded in this study (see Section 4.2). B= Base, T=Top, C=Common.

3.2. Magnetic susceptibility (MS) measurements

Magnetic susceptibility measurements were taken directly on the core, using a Bartington MS2E1 sensor (sensitivity of 2×10^{-6} SI). The uppermost Sinemurian-lowermost Toarcian interval (from 440.0 to 360.0 m) was measured every 2 cm (Fig. 2). The intervals 360-336.0 m and 336.0-194.55 m were previously measured by Boulila et al. (2014) with an even step of 2 and 4 cm, respectively. A total of 8852 MS measurements have been conducted along the 245.45 m thick record.

3.3. Time series analysis

We analyzed in detail the MS data of the latest Sinumerian through the latest Pliensbachian (from 325 to 440 m). The long-term irregular trends in MS variations were measured and subtracted using the weighted average LOWESS method. These data were resampled to the thinnest sampling interval of 2 cm, then linearly interpolated prior to spectral analysis. For spectral analysis, we used the multitaper method (MTM, Thomson, 1982) associated with the robust red noise modelling as implemented in the SSA-MTM Toolkit (Ghil et al., 2002). Spectral analysis was first applied per short intervals, jointly with a manual use of frequency ratio method (e.g., Huang et al., 1992; Mayer and Appel, 1999; Boulila et al., 2008) to recognize Milankovitch cycle bands, and assess potential changes in sedimentation rate.

Then, we statistically assessed changes in sedimentation rate using the evolutive harmonic analysis (EHA) (Meyers et al., 2001). Finally, we applied the COCO method (the

correlation coefficient method, Li et al., 2018) to statistically check our visual interpretation (inspection) of Milankovitch cycle bands. The COCO technique is an automatic frequency ratio method inspired from the average spectral misfit (ASM) of Meyers and Sageman (2007). It estimates the correlation coefficient between the power spectra of an astronomical target signal and paleoclimate proxy series across a range of tested sedimentation rates. As with ASM, a null hypothesis of no astronomical forcing is evaluated using Monte Carlo simulation.

For orbital tuning, we extracted the 405 kyr (g2–g5) MS related eccentricity cycles using bandpass Gaussian filtering (Paillard et al., 1996), and the *depth-to-time* Matlab script (Li et al., 2018) to calibrate the related g2–g5 wavelengths to a pure 405 kyr period on the basis of a minimal tuning (e.g., Muller and MacDonald, 2000). The composite 405 kyr tuned MS signal has then been resubmitted to spectral analysis to look for other aligned, calibrated Milankovitch frequencies. These 405 kyr tuned MS frequencies were compared to the theoretical astronomical periodicities of the considered geologic period (Laskar et al., 2004, 2011). Finally, the 405 kyr tuned MS time series of the latest Sinumerian through the latest Pliensbachian, combined with the cyclostratigraphic results of the latest Pliensbachian through the earliest Aalenian from a previous study (Boulila et al., 2014) were used to study long-period (Myr to multi-Myr) Milankovitch cycles. Here we used the Singular Spectrum Analysis (SSA) method (Ghil et al., 2002) together with bandpass filtering to isolate low-frequency bands. SSA method separates signals from noise in a sequence of signal components (reconstructed components, RCs) that are statistically independent, at zero lag, and based on signal strength (variance).

4. Results

4.1. Ammonite biostratigraphy

An ammonite biozonation of the core was initially established by Lorenz et al. (1987, 1991). Few identifications provided by Lorenz et al. (1987) have been changed because the compression of the specimens or the inaccessibility to shape of the whorl section and ventral area do not allow an accurate identification at the species level, or more rarely, because it was erroneous. This is particularly the case for the species belonging to *Aegoceras*, *Oistoceras*, *Amaltheus* and *Pleuroceras* genera (Fig. 3). However, this reappraisal does not deeply modify the biochronological framework used in the previous studies (Lorenz et al. 1987, Peti et al. 2017). At the Biozone level, our results are fully congruent with these studies. But, it seems to us that *Gibbosus* ammonite Subzone is difficult to characterize (Fig. 2). The only specimen of *A. gibbosus* identified by Lorenz et al. (1987) at 374.9 m appears to be closer to *A. sunodosus* than to *A. gibbosus* (Fig. 2). The base of *Subnodosus* ammonite Subzone is then defined at 394.56 m after the last occurrence (LO) of *A. stokesi* (394.82 m) and the top at 374.88 m at the LO of *A.* cf. *subodosus.* The identification of the *Gibbosus* ammonite Subzone seems unreliable based on the available specimens. The transition between *Margariatus* and *Spinatum* ammonite Zones lies between the LO of *A. margaritatus* at 366.95 m and the first occurrence (FO) *of Pleuroceras* cf. *solare* at 366.25 m. Levels from 266.25 and 355.8 m show a *Pleuroceras* fauna, with all specimens included in either the variability of *P. spinatum* or *P.solare,* typical of the Apyrenum ammonite Subzone (Fig. 2). No ammonites provide any evidence of the *Hauwkerense* Subzone.

4.2. Calcareous nannofossil biostratigraphy

Sancerre calcareous nannofossil assemblages are overall well preserved and abundant (Fig. 4). The main calcareous nannofossil bio-horizons useful for biostratigraphy are summarized in Table 1 (B= base; T= top; C= common occurrence) and their base, top and common occurrence are calibrated with the ammonite zones and sub-zones established in this work. We did not make use of any of the zonal schemes available for this time interval (for example, see Bown and Cooper, 1988 for the boreal realm or Mattioli and Erba, 1999 for the Tethyan realm) for three main reasons: i) these zonal schemes are composed by a succession of datums (First occurrence, last occurrence) and thus, we prefer to focus on the reliability of the datum (biohorizon) itself. ii) New zone and subzone emendations (e.g. Ferreira et al., 2019) and/or regional zonations (Fraguas et al., 2015) recently proposed may create confusion in the correlation of the nannofossil zones. iii) the Sancerre core bears a mixed Boreal-Tethyan assemblages. The calcareous nannofossil succession found at Sancerre is composed by first and last occurrences of index species comparable with those found in both the Boreal Realm (Bown and Cooper, 1998) and low-latitude Tethyan zonations (Mattioli and Erba, 1999), although some biohorizons can be diachronous from a realm to another. Calcareous nannofossil biostratigraphy of the interval from 513 to 410 m can be found in Peti et al. (2017).

4.3. Time-series analysis in the depth domain

Spectral analysis per intervals of MS data jointly with manual use of frequency ratio method and visual inspection of MS variations indicate four distinct sedimentation rate intervals: roughly I1 (360–325 m), I2 (369–355 m), I3 (415–362 m), and I4 (440–412 m) (Fig. 5). Interval I1 shows two low-frequency peaks of 7.25 and 1.84 m. At high-frequency band, there are several peaks, in particular those with wavelengths of 1.84, 0.98, 0.8-0.54, 0.35-0.22, and 0.18-0.13 m (Fig. S1A). Frequency ratio method and visual inspection of MS data indicate a ratio of 1/4 for the 1.84 over 7.25 m sedimentary cycles, matching respectively the short (100 kyr) and 405 kyr eccentricity cyclicities. Frequency ratios also indicate that wavelengths 0.54 through 0.8 m match the obliquity cycles, and wavelengths 0.13 through 0.35 m may correspond to the precession periods.

Interval I2 shows two strongest, low-frequency peaks of 3.33 and 0.83 m. Visual inspection of MS data show prominent bundling of the 0.83 m wavelength by the 3.33 m one (Fig. S1B). High-frequency peaks (0.12 through 0.33 m) are recorded with small MS oscillations. Frequency ratios suggest that the 3.33 m wavelength may match the 405 kyr eccentricity, and the 0.83 m may correspond to the short eccentricity (Fig. 6). The high-frequency, small MS swings match possibly the precession and obliquity cycles.

Interval I3 shows five low-frequency peaks: 7.41 m, 3.13 m, 1.94 m, 1.58 m and 1.21 m (Fig. S1C). There are also several peaks at high frequencies, which can be subdivided into three bands: 0.53-0.76, 0.25-0.45, and 0.13-0.18 m. Frequency ratios and visual inspection of MS data indicate that the 7.41 m wavelength may record the 405 kyr eccentricity, and the 1.58 and 1.94 m may represent the short eccentricity. The bands of 0.53-0.76, 0.25-0.45 and 0.13-0.18 m may match respectively the obliquity, precession and sub-precession bands.

Interval I4 shows three low-frequency peaks of 4.95, 1.64 and 1.20 m (Fig. S1D). Higher frequency peaks of 0.42, 0.27 m and several others from 0.22 to 0.12 m are characterized with elevated powers. The 4.95 m cyclicity bundles almost three 1.64 m cycle repetitions, and the 1.64 m cyclicity bundles four 0.42 m cycle repetitions (Fig. S2). We interpreted the 1.64 m wavelength as corresponding to the 405 kyr eccentricity, and the 0.42 m wavelength as the short eccentricity (Fig. 6). Thus, the 4.95 m cyclicity would have a 1.2

Myr period (three 405 kyr cycle repetitions). This cyclicity has also been documented in the Cenozoic (e.g., Galeotti et al., 2010; Boulila et al., 2018), but its astronomical origin is not yet determined. Peaks from 0.12 to 0.27 m would represent the obliquity band.

The above cyclostratigraphic interpretations were reinforced using EHA and COCO results. EHA of the whole studied interval roughly captures the four intervals I1 through I4 (see spectral line in Fig. 5). COCO outputs per intervals reveal optimal sedimentation rates that are consistent with results from visual inspection of MS cycles (Fig. 7).

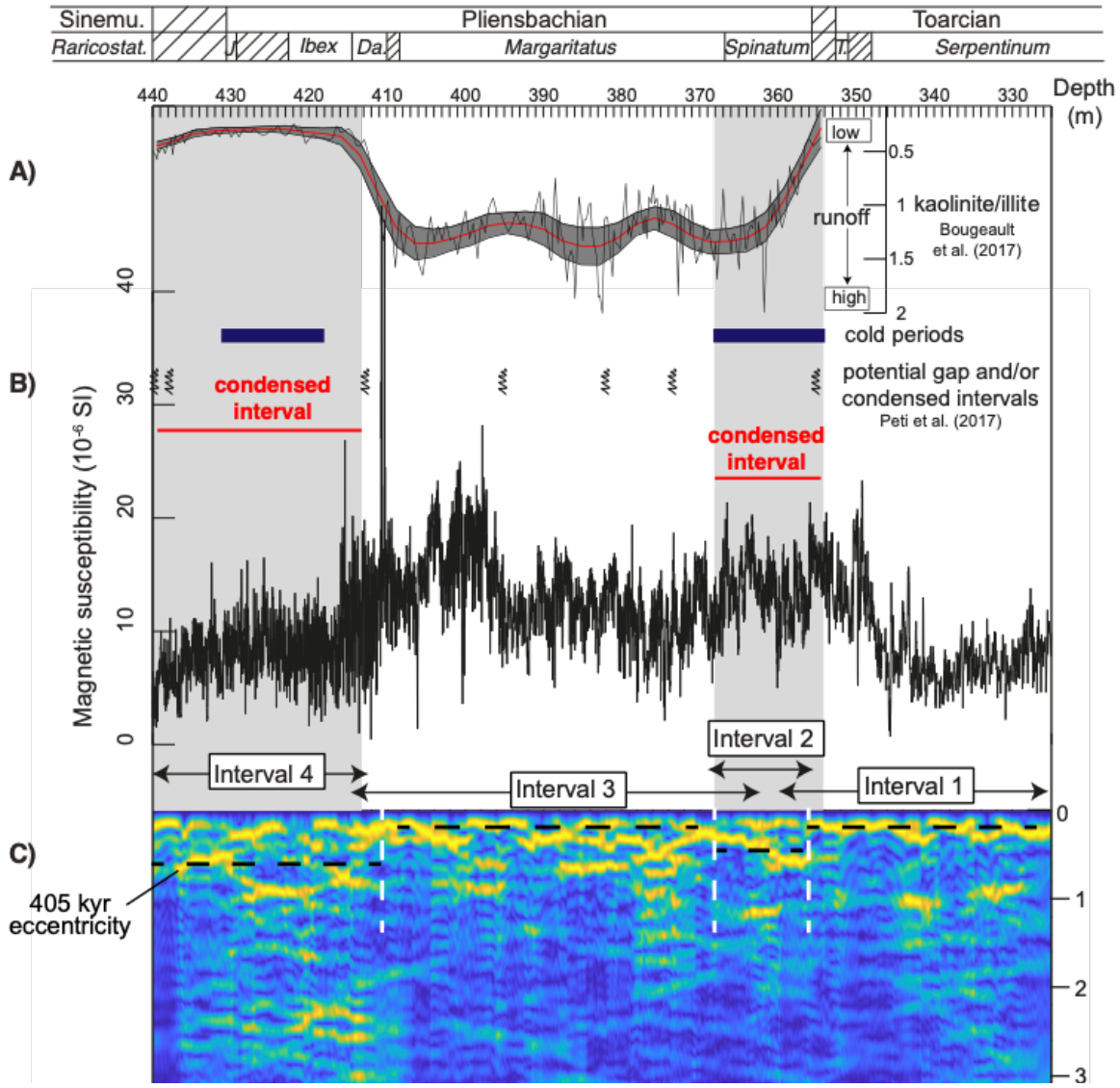

Fig. 5: Latest Sinemurian-earliest Toarcian integrated biostratigraphy, clay mineralogy, sedimentology, and magnetic susceptibility (MS) along with evolutive Fast Fourier Transform (FFT) applied to detrended MS data. **(A)** Summary of clay-mineral and sedimentological data, with kaolinite/illite ratio as a proxy of continental runoff and humidity/aridity changes (Bougeault et al., 2017), with blue intervals corresponding to cold periods based on $d^{18}O$ belemnite dataset (Bougeault et al., 2017), along with potential condensed intervals based on bio- and chemostratigraphy data (Peti et al., 2017). **(B)** Detrended MS variations with a 30% weighted average of the series. **(C)** Evolutive FFT analysis of the detrended MS record (8 m

moving window width, and 0.2 m step). Horizontal, dashed black lines roughly indicate mean wavelengths of each change in the spectral line related to the 405 kyr eccentricity cycle.

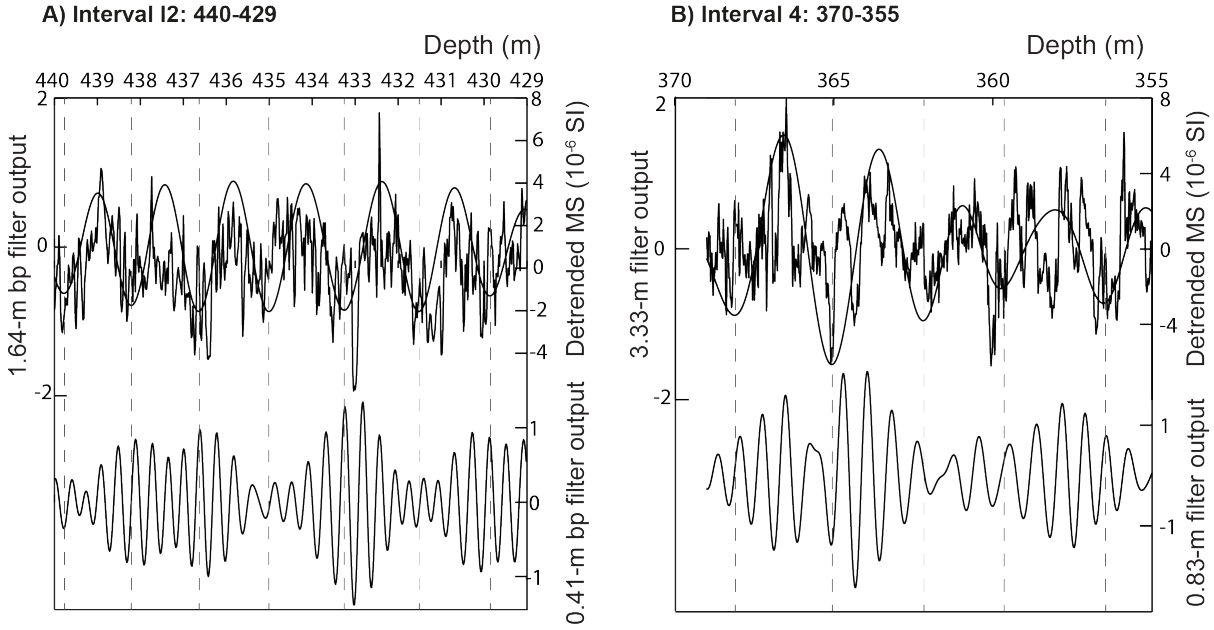

Fig. 6: Detail on cycle interpretation of the Pliensbachian interval. (**A)** Detrended MS data from 440 to 429 m along with 0.41 and 1.64 m bandpass filters using cutoff frequencies 2.31 and 2.61 cycles/m, and 0.56 and 0.66 cycles/m respectively. Note that the 1.64 m bandpass filter is not at the same scale of the detrended data. The 0.41 and 1.64 m peaks are interpreted as reflecting the short eccentricity and 405 kyr eccentricity cycles, respectively. (**B)** Detrended MS data from 370 to 355 m along with 0.83 and 3.33 m bandpass filters using cutoff frequencies 1.1855 and 1.4855 cycles/m, and 0.15 and 0.45 cycles/m respectively. Note that the 3.33 m bandpass filter is not at the same scale of the detrended data. The 0.83 and 3.33 m peaks are interpreted as reflecting the short eccentricity and 405 kyr eccentricity cycles, respectively. Power spectra of these data are shown in Fig. 5 (intervals 2 and 4).

4.4. Time-series analysis in the time domain

Wavelengths reflecting the 405 kyr (g2–g5) eccentricity component were bandpass filtered, then tuned to a pure 405 kyr sinusoid (Fig. S4). Such tuning results in a duration of 12.38 Myr for the studied interval, spanning the latest Sinemurian through the earliest Toarcian (Fig. S3). Spectral analysis of the 405 kyr tuned MS time series of the studied interval shows two dominant peaks of 1.6 and 3.4 Myr (Fig. S4). Other high-frequency bands can be attributable to the short eccentricity, obliquity and precession cycle bands. Spectral analysis of a longer time interval combining the studied interval with the Toarcian Stage (Boulila et al., 2014) also detects the two dominant peaks of 1.6 and 3.4 Myr (Fig. S5). SSA results further support the 1.6 and 3.4 Myr MS cyclicities. We should also note that the powers of 1.6 and 3.4 Myr cycles are focused on the upper part of Pliensbachian through the Toarcian stage (Fig. 8). Additionally, two and a half large amplitude MS oscillations of a periodicity ranging from 7 to 8 Myr could be extracted by the SSA method, although its precise periodicity cannot precisely be quantified because of the lack of cycle repetitions. This cyclicity match the timing of the global eustatic sequences of Haq et al. (1987) (see Section

5.3). The 1.6 Myr MS cycle was interpreted as reflecting the g4–g3 eccentricity term during the Toarcian stage (Boulila et al., 2014). The prominent 3.4 Myr cyclicity, which has been evoked in Boulila et al. (2014), will also be investigated in more depth in the present study as likely corresponding to a longer eccentricity term (Boulila, 2019; Boulila et al., 2020). Therefore, we will discuss the potential use of both the 1.6 and 3.4 Myr eccentricity terms as indicators of the chaotic diffusion in the inner Solar System (Section 5.2). Finally, the persistence of the 1.6 Myr cyclicity during the Toarcian and Pliensbachian stages and its potential impact on the Early Jurassic sea-level changes will together be discussed in Section 5.3.

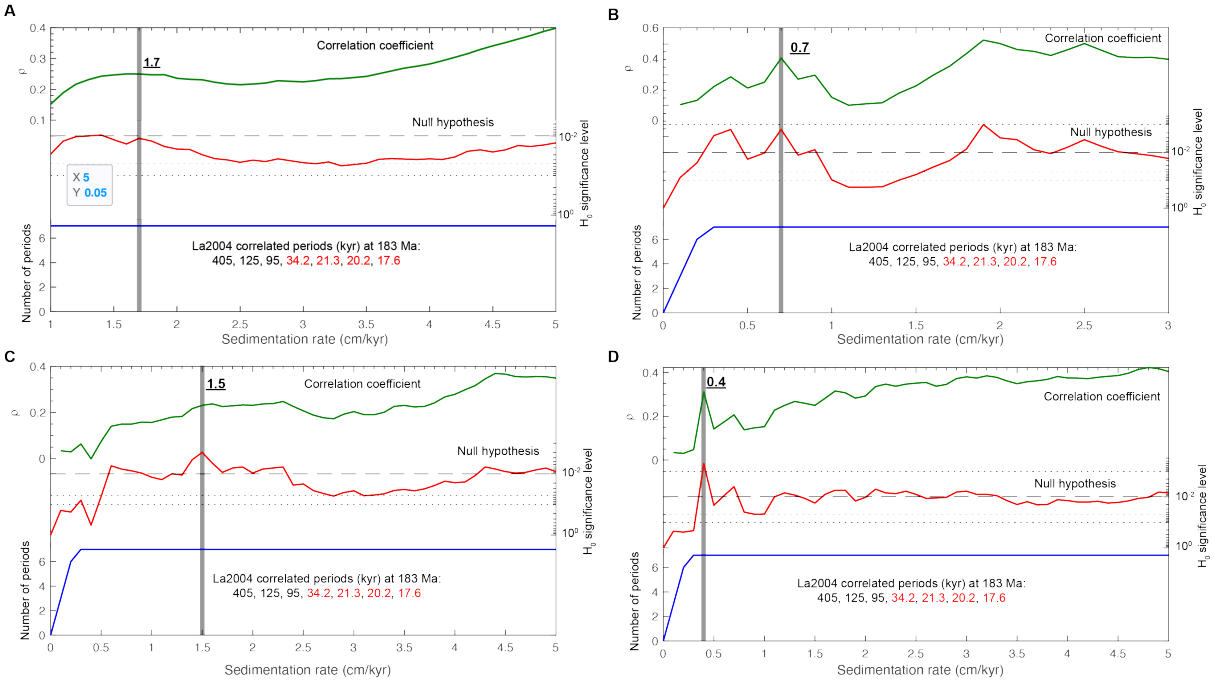

Fig. 7: The COCO results (correlation coefficient method, Li et al., 2018) per intervals, used to statistically check the visual interpretation of Milankovitch cycles bands. (**A)** Interval 1: 360-325 m. (**B)** Interval 2: 369-355 m. (**C)** Interval 3: 415-362 m, and (**D)** Interval 4: 440-412 m). COCO outputs, potential sedimentation rates (green line), the null hypothesis results (red line, H0 significant level), and the number of contributing astronomical parameters in the target in the tested sedimentation rate (blue curve). Null hypothesis of no astronomical forcing is estimated by Monte Carlo simulation with 2000 iterations. The astronomical target series is La2004 astronomical solution from 193.9 to 173.9 Ma (Laskar et al., 2004).

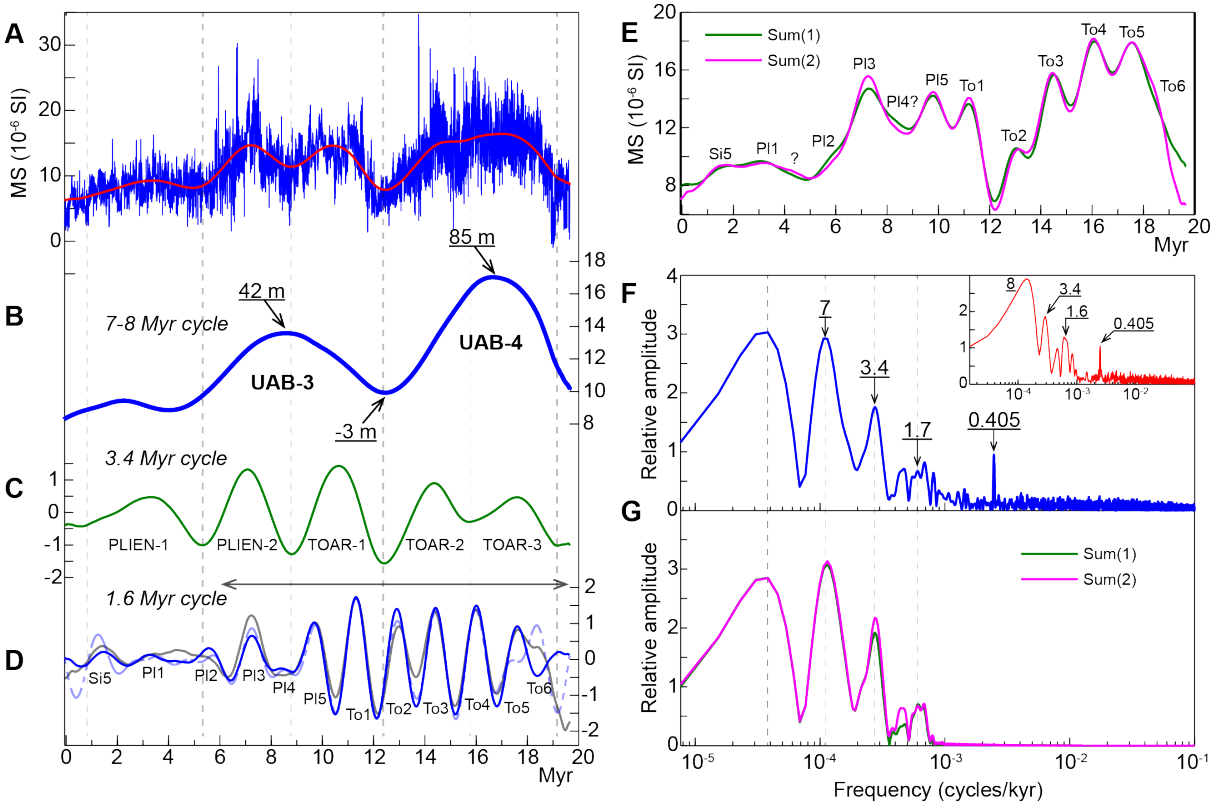

Fig. 8: SSA long-period cycle decomposition of the 405 kyr tuned MS time series. **(A)** Raw MS along with the three SSA first components RC1+RC2+RC3 (M = 1 Myr). **(B)** The two first components RC1+RC2 (M = 5 Myr). **(C)** The third component RC3 (M = 1 Myr). **(D)** The RC4+RC5+RC6 components (M = 1 Myr) (dark blue curve) and RC5+RC6 components (M = 1 Myr) (grey curve) along with and a gaussian bandpass filter (0.616 ±0.2 cycles/Myr) (light blue, dashed curve). **(E)** Sum of the three SSA reconstructions in 'B', 'C' and 'D', in green, *Sum(1)*, only the two SSA RC5+RC6 in 'D' were used, and in pink, *Sum(2),* the three SSA RC4+RC5+RC6 in 'D' were used). **(F)** 2p-MTM amplitude spectrum of raw MS data. *Inset*: only the interval from 7.6 to 19.652 Myr was analyzed. Statistical significance and spectral uncertainty on peaks are shown in figure 9. **(G)** 2p-MTM amplitude spectrum of the composite curve in 'E'. The 7, 3.4 and 1.6 Myr cycles are the three dominant cycles in MS time series.

5. Discussion

5.1. Astronomical calibration of the Pliensbachian stage

The uppermost Sinemurian-lowermost Toarcian age interval of the Sancerre borehole is based on a detailed biozonation by ammonites and calcareous nannofossils (Sections 4.1 and 4.2). Due to some stratigraphic uncertainties in the position of the ammonite zone boundaries we consider two durations (minimal/maximal) for the Pliensbachian stage and ammonite zones (Table 2).

Due to the scarcity of index fossils, the base of the Pliensbachian stage is not precisely identified between the top of the *Raricostatum* zone at 440 m and the base of the *Jamesoni* zone identified at 430.5 m (Lorenz et al., 1987; Peti et al., 2017). The Pliensbachian/Toarcian

boundary is more precisely constrained according to the ammonite bio-horizons (*Spinatum-Tenuicostatum* zones) between 355.8 and 352.8 m (Boulila et al., 2014). Using the 405 kyr tuned MS series, we propose minimal and maximal durations of ~8.74 Myr (from 430.5 to 355.8 m), and ~11.4 Myr (from 440 to 352.8 m) for the Pliensbachian stage. The ~8.74 Myr minimal duration is close to the ~8.7 to ~8.8 Myr duration estimated on the basis of a cyclostratigraphic study (on XRF elemental Ca content, $\delta^{13}C_{TOC}$) from the Mochras borehole (Wales, UK) (Ruhl et al., 2016; Storm et al., 2020) (Table 2). However, this duration is longer than the more recent estimate of ~8.4 Myr inferred from cyclostratigraphy of ichnological data in the same Mochras borehole (Pieńkowski et al., 2021). Additionally, using the 405 kyr timescale we provide durations for the standard ammonite biozones (Table 2).

Table 2

	This study		Ruhl et al., 2016	Storm et al., 2020	Pieńkowski et al., 2021	McArthur et al., 2000	GTS2020
	minima	maxima	elemental Ca	δ13C (TOC)	ichnology		
U. jamesoni	3.91 Myr	6.24 Myr	2.7 Myr	2.4 Myr	2.8 Myr		2.7 Myr
T. ibex			1.8 Myr	1.8 Myr	2.0 Myr		1.8 Myr
P. davoie	0.51 Myr	0.62 Myr	0.4 Myr	0.4 Myr	0.47 Myr		0.4 Myr
A. margaritatus	2.67 Myr	2.78 Myr	2.4 Myr	2.7 Myr	2.33 Myr	2.75 Myr	2.4 Myr
P. spinatum	1.54 Myr	1.87 Myr	1.4 Myr	1.4 Myr	0.8 Myr	1.21 Myr	1.4 Myr
Pliensbachian	8.74 Myr	11.4 Myr	8.7 Myr	8.8 Myr	8.4 Myr		8.7 Myr

Table 2: Comparison of Pliensbachian stage and ammonite zone duration estimates in the Paris Basin (This study), the Cardigan Bay Basin (Mochras, Wales; Ruhl et al., 2016; Storm et al., 2020), and the Yorkshire Coast Basin (strontium isotope data; McArthur et al., 2000), and GTS2020 based on the cyclostratigraphic data of Ruhl et al. (2016) (Gradstein et al., 2020).

Two intervals from 377 to 369 m (end *Margaritatus-Spinatum* zones) and from 440 to 412 m (*Jamesoni-Ibex* zones) are particularly characterized by lower sedimentation rates (Figs 5 and 6). Interestingly, clay mineral assemblage and stable isotope geochemistry data at Sancerre suggest that the *Jamesoni-Ibex* interval and the *Spinatum* zone was marked by the development of cooler conditions associated with low runoff (Bougeault et al., 2017) (Fig. 5). Furthermore, numerous supposedly condensed intervals are indicated by the thickness of nannofossil subzones and the sharpness of the drop in carbon isotope signal in the interval spanning the Sinemurian/Pliensbachian boundary (440-430 m), between the *Ibex-Davoie* zones (412-407.5 m), at the end of the *Margaritatus* zone (375-370 m), and in the *Spinatum* zone (355.05 m) (Peti et al., 2017; This study). These results highlight low sedimentation rates observed in the *Jamesoni*, *Ibex*, end *Margaritatus*, and *Spinatum* zones (Fig. 5). In contrast, the *Davoie* and *Margaritatus* zones are characterized by enhanced humidity and warmer conditions, which appear consistent with higher sedimentation rates (Fig. 5). The minimal and maximal durations for the combined *Jamesoni-Ibex* zones are assessed at ~3.91 and ~6.24 Myr. These durations are different from those published from the Mochras borehole, who reported a duration between ~4.2 and ~4.8 Myr, respectively, for the combined *Jamesoni-Ibex* zones (Ruhl et al., 2016; Storm et al., 2020; Pieńkowski et al., 2021) (Table 2). This difference in terms of durations between cores (~3.91 vs ~4.2) may be explained by the large uncertainties in the definition of the boundaries of biohorizons and/or by the presence of hiatuses in the interval spanning the Sinemurian/Pliensbachian boundary (Peti et al., 2017). The minimal duration of the *Davoie* zone obtained in this study (~0.51 Myr) is close to that proposed by Ruhl et al. (2016) and Storm et al. (2020) (~0.4 Myr), and Pieńkowski et al. (2021) (~0.47 Myr). The *Margaritatus* ammonite biozone at Sancerre spans ~2.67 Myr (minimal) and ~2.78 Myr (maximal). These durations are more or less in agreement with previous studies at Mochras (~2.4 Myr, Ruhl et al., 2016; ~2.7 Myr, Storm et al., 2020).

However, our duration estimate of the *Margaritatus* zone (~2.67 to ~2.78 Myr) is much longer than that inferred from ichnological cyclostratigraphy (~2.33 Myr; Pieńkowski et al., 2021). Our estimation is also consistent with that of McArthur et al. (2000) (~2.75 Myr) based on an independent approach (isotopic trends in $^{87}Sr/^{86}Sr$). Interestingly, the duration of the *Jamesoni-Margaritatus* interval at Sancerre (~7.2 Myr) is very close to the ~7.3 Myr estimate from Mochras using Ca and $\delta^{13}C_{TOC}$ cyclostratigraphies (Ruhl et al., 2016; Storm et al., 2020) but shorter than that inferred from ichnological cyclostratigraphy (~7.6 Myr; Pieńkowski et al., 2021). Finally, the minimal duration of the *Spinatum* zone at Sancerre is assessed at ~1.54 Myr (minimal) and ~1.87 Myr (maximal). The minimal duration is somewhat close to the ~1.4 Myr estimate at Mochras (Ruhl et al., 2016; Storm et al., 2020). However, it is longer than the ~0.8 Myr and ~1.21 Myr durations proposed by Pieńkowski et al. (2021) and McArthur et al. (2000), respectively (Table 2).

In summary, our results suggest that despite the occurrence of some intervals with low sedimentation rates, in particular in the lowermost and uppermost Pliensbachian, the sedimentary succession at Sancerre is likely continuous (Fig. 5).

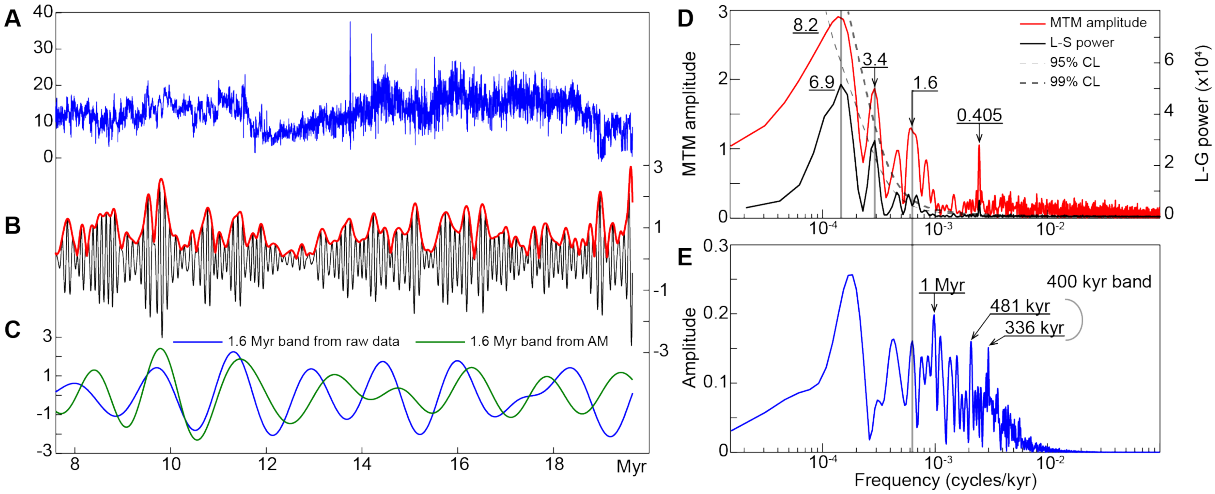

Fig. 9: Amplitude modulation (AM) analysis of the short eccentricity band. **(A)** 405 kyr tuned, raw MS series of the interval from 7.6 to ~20 Myr (upper part of Pliensbachian through the basal Aalenian). **(B)** Short eccentricity bandpass filter output (0.01 ±0.003 cycles/kyr) and Hilbert-transform output. **(C)** 1.6 Myr bandpass filter outputs (0.0006 ±0.0002 cycles/kyr) from the raw data (blue) and from AM envelopes (green). **(D)** 2π-MTM amplitude spectrum and Lomb-Scargle (L-S) peridogram of the tuned raw MS data in 'A'. **(E)** 2π-MTM amplitude spectrum of the AM envelopes in 'B'. Note that the 1.6 Myr peak is split into two peaks of 1.5 and 1.7 Myr in L-S periodogram because L-S method discretizes, while the MTM does not. Spectral uncertainties on the 1.6 and 3.4 Myr peaks are ±0.1 and ±0.4 Myr respectively.

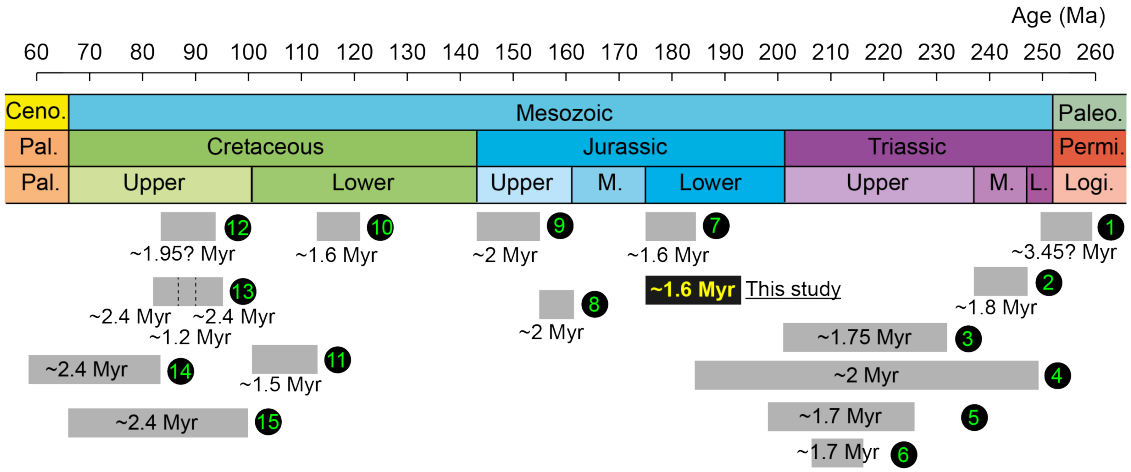

Fig. 10: Main cyclostratigraphic secquences recording the long-term eccentricity orbital cycle (term g4-g3) during the Mesozoic. 1: Wu et al., 2013a, 2: Ikeda et al., 2010, 3: Olsen and Kent, 1999, 4: Ikeda and Tada, 2014, 5: Olsen et al., 2019, 6: Mau et al., 2022, 7: Boulila et al., 2014, 8: Boulila et al., 2010, 9: Huang et al., 2010a, 10: Huang et al., 2010b, 11: Grippo et al., 2004, 12: Wu et al., 2013b, 13: Ma et al., 2019, 14: Herbert, 1999, and 15: Boulila et al., 2020. Periodicities of the long-eccentricity term are reported in age according to GTS2020 (Gradstein et al., 2020).

5.2. Expression of planetary chaotic motions in long-period eccentricity cycles

The chaotic nature in the inner Solar System has been demonstrated by showing an important value of the Lyapunov exponent (Laskar, 1989), which is an eigenvalue to describe a chaos system (Wolf, 1986). Thus, the high value of the Lyapunov exponent was then related to the presence of secular resonances in the inner Solar System, where the origins of several resonances were detected (Laskar, 1990; Lithwick and Wu, 2011; Magavero and Laskar, 2022). In particular, an important resonant argument was highlighted, called q = 2(g4 – g3) – (s4 – s3) (Laskar, 1990). This argument includes two long-period orbital periodicities g4–g3 in the eccentricity, and s4–s3 in the obliquity, with their respective Cenozoic mean values of 2.4 and 1.2 Myr. These mean periods could deviate in deeper geological times, in the Mesozoic for example, due to the chaotic behavior of the orbital motion in the inner Solar System (Laskar, 1989, 1990, 2020; Laskar et al., 2011; Hoang et al., 2021). Thus, geological records of these long-period orbital cyclicities can provide a good opportunity to test theoretical astronomical solutions, and to detect features of the potential chaos (e.g., Olsen and Kent, 1999; Boulila et al., 2010, 2014; Wu et al., 2013a; Ma et al., 2017; Olsen et al., 2019; Mau et al., 2022). The highly resolved MS dataset at Sancerre, tuned to the 405 kyr stable eccentricity cycle (Sections 4.2 and 4.3), allows to establish a ~20 Myr long cyclostratigraphic record of Early Jurassic age (174-194 Ma, according to GTS2020, Gradstein et al., 2020). This 405 kyr calibrated MS record shows evidence for long-period cyclicities of ~1.6 and ~3.4 Myr (Fig. 8). These two cyclicities likely correspond to the 2.4 and 4.7 Myr eccentricity terms (Cenozoic values). This hypothesis is further supported by amplitude modulation (AM) analysis of the short eccentricity band, which captures the 1.6 Myr modulator cycles (Fig. 9). Additionally, we can observe almost four g2–g5 related oscillations in each well-expressed 1.6 Myr cycle (Fig. 8). The 2.4 Myr (g4–g3) eccentricity term has been documented in numerous Cenozoic and Mesozoic cyclostratigraphic records. However, the 4.7 Myr eccentricity term has been rarely detected in the geological records

(Boulila et al., 2012). It has been recently detected in Cenozoic climatic record (Boulila, 2019), and in Late Cretaceous sequences in the Foz do Amazonas Basin (Boulila et al., 2020). The astronomical origin of this geologically recorded 4.7 Myr cycle has been attributed to the libration period of the resonant argument q = 2(g4-g3)-(s4-s3) (Boulila et al., 2020). Thus, the Sancerre record may show significantly shortened 2.4 and 4.7 Myr periodicities, i.e. 1.6 and 3.4 Myr respectively (Fig. 8), which possibly reflect the chaotic orbital motion of the inner planets (Laskar, 1989) during the Early Jurassic.

Several Mesozoic cyclostratigraphic studies pointed to a shortened g4–g3 eccentricity, except for the Late Cretaceous, during which it should have the same Cenozoic value (i.e., 2.4 Myr) (Fig. 10). In particular, recent studies of the Late Triassic to earliest Jurassic highlighted a mean periodicity of 1.7 Myr (Olsen et al., 2019; Mau et al., 2022), thus concuring with the Early Jurassic Paris Basin record for a shortened g4–g3 eccentricity term.

In addition to their implication for the potential chaos in deeper geological times, these Early Jurassic 1.6 and 3.4 Myr periodicities may have also played an important role in the global sea-level changes (Boulila et al., 2014, Section 5.3).

5.3. Impact of long-period orbital cycles on sea-level (SL) changes

SL changes in the Paris sedimentary Basin and the surrounding margins may have played a major control on the deposition of terrigenous clastics (mainly clays) and marine carbonate production, as reflected by the MS dataset (e.g., Boulila et al., 2014). The Paris Basin has received a particular interest for Mesozoic sequence stratigraphy since 1990's, because it was a sensitive area to climatic changes modulated by tectonic evolution of the Tethyan and Atlantic Oceans (e.g., Guillocheau, 1991; Guillocheau et al., 2000). It was also used to contribute to building the reference NW European eustatic chart (Hardenbol et al., 1998; Jacquin et al., 1998; de Graciansky et al., 1998). The eustatic charts, which are representations of hierarchical SL related depositional sequences, have long been used by geologists for global stratigraphic correlations. In particular, SL sequences and their causal mechanisms have been the focus of researchers since 1980's, such as the pioneers of Exxon Production Research Company (Vail et al., 1977; Haq et al., 1988; Haq et al., 1987; Simmons, 2012; Simmons et al., 2020).

Duration of SL sequences is a fundamental criterion for the definition of the hierarchical order, hence for the suggested driving mechanism (e.g., Simmons, 2012; Simmons et al., 2020). There is increasing evidence from very long (Muti-Myr) cyclostratigraphic and SL proxy records for the link between global third-order (Myr-scale) depositional sequences, and long-period Milankovitch cycles (e.g., see Boulila et al., 2011 for a review).

In particular, correlations of third-order SL sequences and g4-g3 eccentricity term in the Paris Basin Toarcian stage show a strong correspondence between the two, suggesting that orbital eccentricity forcing is the main driver of climate and SL changes at this frequency band (Boulila et al., 2014). Here we explored this hypothesis for the Pliensbachian Stage. We also looked for much longer cyclicities within the ensemble of Pliensbachian and Toarcian stages.

The Pliensbachian Stage contains five and a half to six and a half g4-g3 eccentricity related cycles (Fig. 8). Such uncertainty is due to the poorly defined basal boundary of the Pliensbachian Stage (Section 5.1). Thus, comparison between g4-g3 MS cycles and third-order sequences (Hardenbol et al., 1998) is not straightforward. Then, we focused on the well-dated interval of the Pliensbachian, i.e. the interval spanning the three ammonite zones *Davoie, Margaritatus*, and *Spinatum*. This interval includes almost four g4-g3 MS related cycles versus five and a half third-order eustatic sequences in the European reference chart

(Hardenbol et al., 1998). Three among these sequences were considered as minor sequences, and the two and a half other ones were interpreted as medium sequences. Again, a potential link between g4-g3 related cycles and third-order sequences could not be established even within the above, biostratigraphically well-dated interval.

Indeed, as mentioned in previous studies (Boulila et al., 2011, 2010, 2014), the eustatic reference chart sometimes presents a mixture of frequency bands attributed to the same order (i.e., third order). For instance, the minor and medium third-order SL sequences may represent a mixture of 405 kyr and 2.4 Myr eccentricity forcings, thus pointing to the difficulties in providing a consistent SL hierarchy, mainly due to the lower stratigraphic resolution. Combining cyclostratigraphy and sequence stratigraphy should place SL sequences in a precise temporal timescale, hence constraining their hierarchy.

The Sancerre MS record documents short- and long-term cyclic variations in carbonate versus clay deposition in the Paris Basin (Boulila et al., 2014; Boulila and Hinnov, 2017). These depositional cycles were modulated by orbitally paced climate and SL changes. In particular, the Sancerre record captures two and a half large MS oscillations encompassing nearly the Toarcian and the Pliensbachian stages (Fig. 8). These two long-period (7-8 Myr, Fig. 8F,G) MS oscillations match the global, "shorter" second order SL sequences (Boulila et al., 2018, 2020) of Haq et al. (1987) (see also Haq, 2018 for an update, Fig. 8B). These second-order sequences have a Cenozoic mean periodiciy of 9.5 Myr, and they likely correspond to a very long-period orbital cycle (Boulila et al., 2012, 2018, 2020; Sprovieri et al., 2013; Martinez and Dera, 2015; Boulila, 2019). Superimposed on these large-scale cycles are the two well-detected, MS cycle bands of mean periodicities of 3.4 and 1.6 Myr (Section 5.2, Fig. 8). The 3.4 Myr cycle has no equivalent SL order (Boulila et al., 2020), while the 1.6 Myr cycle presumably corresponds to third-order sequences. Major changes in ichnodiversity interpreted as oceanographic changes controlled by orbital cycles is observed in the Mochras borehole (Pieńkowski et al., 2021), which correspond laterally to the boundary of long-period oscillations (7-8 Myr) in the Sancerre core. Our results suggest an update of Early Jurassic SL sequence hierarchy, especially at the third-order timescale, based on the reference, Paris Basin Sancerre record (Fig. 8). Although we point to a global SL control of MS related depositional sequences, discussion of the mismatch, at third-order time scale, between Sancerre sequences and the global eustatic sequences (e.g., Haq, 2018) requires further investigation in the future by correlating the Sancerre sequences with cyclostratigraphically highly-resolved sequences from other distant basins. In contrast, the longer MS sequences (7-8 Myr) are seemingly global since they biostratigraphically match the global SL sequences UAB-3 and UAB-4 of Haq et al. (1987) (Fig. 11).

5.4. Sedimentological expression of SL changes in the Paris Basin

The Sancerre core lithology is mainly composed of clays and carbonates. Changes in these lithologies are observable in the core at longer interval, especially at the longer orbital cyclicities (1.6, 3.4 and 7-8 Myr). Highly resolved MS dataset faithfully detects these changes (Fig. 11), with magnetic hysteresis experiments indicating a strong paramagnetic signal from clays, likely diluted by carbonate calcium (Boulila et al., 2014). Carbonate content data of the early Pliensbachian through the earliest middle Toarcian (Hermoso et al., 2012; Peti et al., 2021, Fig. 11D) show significant variations, ranging from ~10 to ~90% (Fig. 11D), reinforcing the idea of the relative contribution of clays and carbonates in the lithological changes (Boulila and Hinnov, 2017). In particular, the long trends (7-8 Myr-scale) in MS data, which are ascribed to orbitally forced climate and SL changes (Section 5.3), can also be captured by clay mineralogy (Bougeault et al., 2017) as well as long-term changes in sedimentation rates deduced from cyclostratigraphy (esp. through intervals with low

sedimentation rates, called here condensed intervals). The lower part of Pliensbachian is characterized by lower kaolinite/illite ratio, higher carbonate content and a condensed interval, in support with colder/drier climatic conditions (Bougeault et al., 2017; Peti et al., 2021) and lower SL (e.g., Haq et al., 1987; Haq, 2018). A strong increase in kaolinite/illite ratio at *Davoie* and basal *Margaritatus* ammonite zones was accompanied by higher clay contents, thus reflecting a warming trend and a SL rise (e.g., Haq et al., 1987; Haq, 2018). A detailed sedimentological description of the core indicates a very dark, clay-rich interval at 413.8-m depth, situated in the inflection point of the strong increase in kaolinite/illite ratio. This interval is characterized by higher MS values (Fig. 2), corroborating for the substantial warming, towards more humid conditions, likely resulting in accelerated rates of continental weathering (Bougeault et al., 2017). The middle part of the Pliensbachian, i.e., basal *Margaritatus* Zone, shows greater kaolinite/illite ratios, higher clay contents, and a negative $d^{18}O$ trend recording warmer climatic conditions and higher SL (Bougeault et al., 2017; Peti et al., 2021). A kaolinite-rich interval coeval to a decrease in carbonate contents also concomitant to significant SL rise (Haq, 2018) is also documented in the *Davoie* and basal *Margaritatus* ammonite zones in the Cardigan Bay Basin at Mochras (Deconinck et al., 2019; Ullmann et al., 2022). Such substantial SL rise in the Cardigan Bay Basin are correlated to reduced ichnodiversity indicative of high atmospheric pCO_2, elevated temperatures and Tethyan warm saline-water influx (Pieńkowski et al., 2021), supporting the sedimentological expression of SL changes at Sancerre.

The upper part of the Pliensbachian and the basal Toarcian (i.e., *Spinatum* and *Tenuicostatum* zones) show significant decrease in kaolinite/illite ratio and a shift in $d^{18}O$ values, coeval to an increase in carbonate content together with a condensed interval, revealing together a climatic cooling (Bougeault et al., 2017; Ruebsam et al., 2019; Peti et al., 2021) and a prominent SL fall (Haq et al., 1987; Haq, 2018). This interval ends with a dm scale ammonite accumulation layer within the *Tenuicostatum* Zone (Boulila and Hinnov, 2017), and a dolostone event likely occuring at the Paris Basin scale (Ruebsam et al., 2014) (Fig. 2). A sea-level drop concomitant to a cooling event during this time interval is also documented in the Lorraine Sub-Basin with higher Si/Al ratios (Ruebsam et al., 2019). The abundance of mixed layer clay mineral associated to carbonate enriched interval and the presence of berthierine at the top of the Pliensbachian are also interpreted as reflecting SL fall and climate cooling in the Cardigan Bay Basin (Deconinck et al., 2019; Ullmann et al., 2022). A smectite-rich interval is associated to higher ichnodiversity linked to limited competition from the opportunist species (i.e. Phycosiphon) (Pieńkowski et al., 2021), which is also consistent with the sedimentological expression of SL drop at Sancerre. During the *Margaritatus-Spinatum* Zones, long $\delta^{13}C$ trends have been attributed by Ruebsam and Al-Husseini (2021) to global changes in atmospheric CO_2 levels and synchronous climate, SL, and glacio-eustatic changes supporting our interpretation.

Low-resolution carbonate content of early Toarcian through earliest middle Toarcian (Hermoso et al., 2012) shows evidence of climate and SL changes at 405 kyr and 1.6 Myr eccentricity bands (Boulila and Hinnov, 2017 their figure 2). Variations in ratio of quartz to quartz+clay (Qz/(Qz+clay) constitute an independent tool to assess variations in SL (e.g., Williams et al., 2001; Hesselbo, 2008). Qz/(Qz+clay) data (Hermoso et al., 2012) capture trends of the 1.6 Myr oscillations (third-order, Boulila and Hinnov, 2017), and in particular show a positive correlation with carbonate content (Fig. 11), revealing a relationship between climate and SL changes. Greater Qz/(Qz+clay) and carbonate-content values reflect lower SL, assuming the quartz deposits originate from continental weathering during SL lows. This is also reflected by 1.6 Myr MS cycle minima (Fig. 8). A concomitant decline in Si/Al ratio and relatively higher carbonate contents (and decreased MS values) was observed in the Lorraine

Sub-Basin, likely registering a rapid SL rise (> 30 m) followed by a period of high SL during the *Serpentinum* Zone (middle Toarcian) (Ruebsam et al., 2014, 2019).

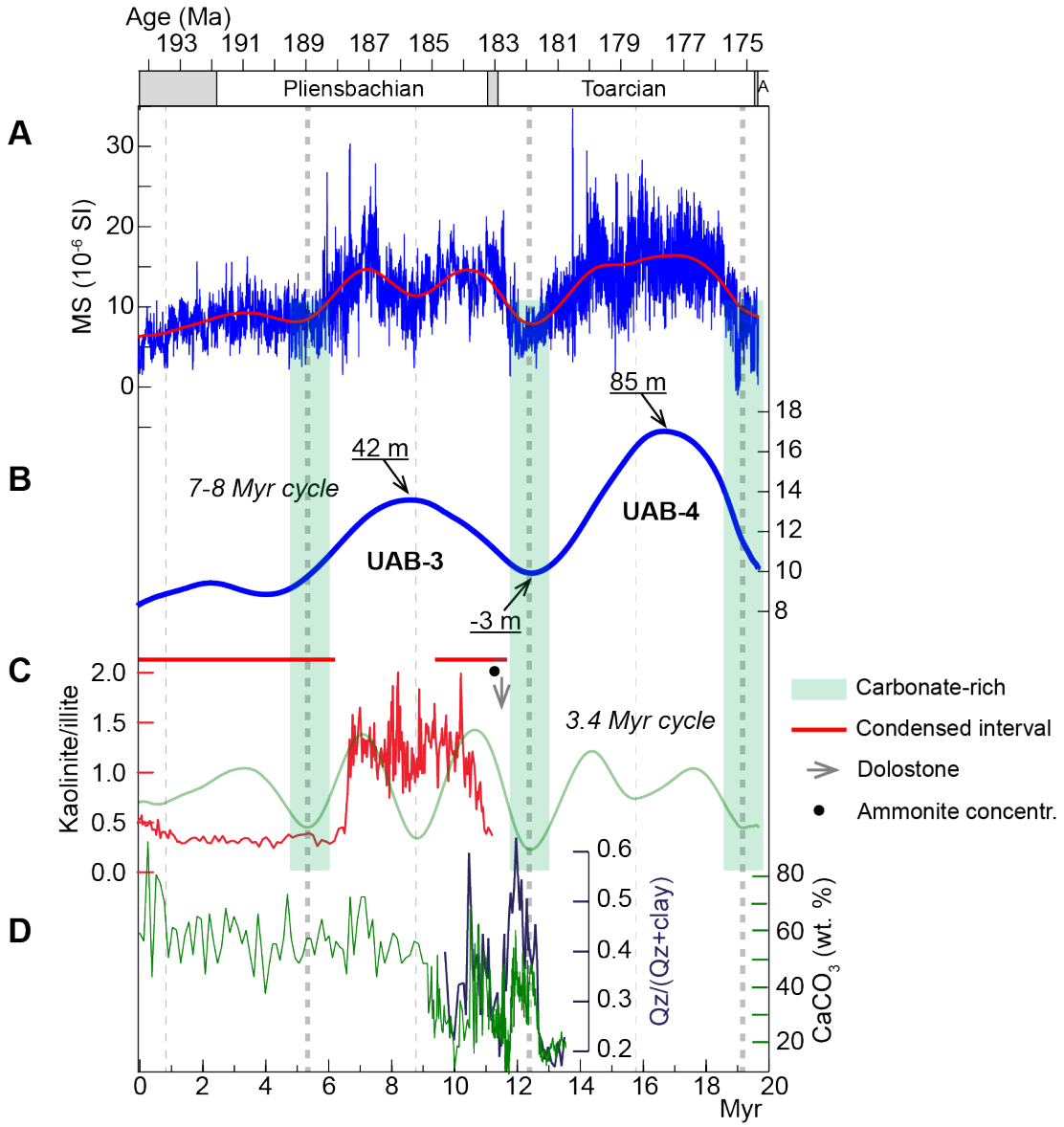

Fig. 11: Expression of long-period climate and SL cycles in MS and mineralogical data. **(A)** MS data and trends as in Fig. 7A. **(B)** 7-8 Myr MS cycles extracted using SSA method (as in Fig. 8B). UAB-3 and UAB-4 eustatic sequences (Upper Absaroka 'B' 3 and 4 of Haq et al., 1987), and their respective amplitudes (relative to present-day SL, Haq, 2018) are indicated. **(C)** Clay mineralogy (red curve, Bougeault et al., 2017), along with 3.4 Myr MS cycles (green curve) and cyclostratigraphically detected intervals with low sedimentation rates (called 'condensed' intervals). Also indicated are the dolostone event (Hermoso et al., 2009), and fossil ammonite accumulation layer (Boulila and Hinnov, 2017). **(D)** Carbonate content (Hermoso et al., 2012; Peti et al., 2021) and Qz/(Qz+clay) data (Hermoso et al., 2013) capturing the 1.6 Myr oscillations.

The expression of the amplitude of the 7-8 Myr MS cycle is variable within the studied interval. It is stronger in the Toarcian than in the Pliensbachian (Fig. 11B). This result is in good agreement with their time equivalent "shorter" second order SL sequences in the global eustatic record (Section 5.3). SL globally dropped from 42 m (relative to present SL) within the Margaritatus Zone to -3 m within the *Spinatum-Tenuicostaum* Zones, then rose up to 85 m in the middle Toarcian (Haq, 2018, Fig. 2). The very low global SL of -3 m at the *Spinatum-Tenuicostaum* Zones may be expressed at Sancerre in the paleontological (accumulation of fossil ammonites) and sedimentological (dolostone event) data (Fig. 2). The prominent changes in sedimentation rates along with the sedimentological responses of the Paris Basin to sea-level change does not reveal the occurrence of hiatuses (Gély et al., 1996). Also, our detailed core description during the process of high-resolution (2 to 4 cm) MS measurements does not show any sedimentological feature, indicator of hiatuses. Despite Peti et al. (2017) have suggested potential hard grounds and marine gully erosions (Figs. 1 and 2), previous reports on Sancerre core (Gély et al., 1996) and our sedimentological description do not show significant erosional surfaces or hiatuses over most of the Pliensbachian-Toarcian interval. One exception is the Pliensbachian-Toarcian transition or rather the top of Pliensbachian, which may be the subject of marine gully erosion, but does not show any biostratigraphic gap (Gély et al., 1996). Previous cyclostratigraphic analyses also suggest potential condensation in the uppermost part of Pliensbachian (Boulila et al., 2014; Boulila and Hinnov, 2017), without evidence for hiatuses. Thus, possible missing time at the condensed intervals may represent only short timespans of thousands of years, and its impact on cyclostratigraphy should be minor as supported by similar durations of correlatable biostratigraphic intervals, e.g. ammonite biozones, among Sancerre and Mochras sites (Section 5.1).

6. Conclusions

High-resolution magnetic susceptibility (MS) measurements for the latest Sinemurian-earliest Aalenian interval at the reference Sancerre core (Paris Basin) exhibit cyclic pattern attributed to Earth's orbital parameters (eccentricity, obliquity, precession). The 405 kyr eccentricicty is well documented in the MS signal, and serves as geochronometer for astronomical tuning. A ~20 Myr long MS cyclostratigraphic record is generated along this key interval. The principal results are:

-A minimal duration of 8.74 Myr is estimated for the Pliensbachian stage, which is close to the duration 8.7 to 8.8 Myr inferred from a cyclostratigraphic approach of the Mochras borehole (Wales, UK).
-The 405 kyr tuned time series shows evidence of long-period cyclicities of ~1.6 and ~3.4 Myr, which likely correspond to the Cenozoic 2.4 Myr (g4–g3) and 4.7 Myr eccentricity terms. These shortened late Jurassic orbital periods may reflect the chaotic orbital motion of the inner planets.
-The Sancerre record captures two long-period MS oscillations (7–8 Myr), matching the "shorter" second order sea level sequences in the global eustatic records. Superimposed on these large-scale cycles are the g4–g3 related eccentricity cycle, presumably corresponding to third order sea level sequences.
-Cyclostratigraphic interpretation and results are supported by sedimentological and clay mineralogical data, which together reinforce the idea that orbital eccentricity forcing is the main driver of climate and sea level changes.

Acknowledgements

We are grateful to editor Dr. Cari Johnson and the Prof. Wolfgang Ruebsam and an anonymous reviewer for their constructive comments and useful suggestions. G.C. has been supported by a grant of the French Agence Nationale de la Recherche (AstroMeso ANR-19-CE31-0002-01). This project has been supported by the European Research Council (ERC) under the European Union's Horizon 2020 research and innovation program (Advanced Grant AstroGeo-885250). We would like to thank Emilia Huret (ANDRA Agency), who helped us in MS data acquisition. We would also like to thank Alexandre Lethiers for diligently drafting Figure 3.

Author Contributions

Magnetic susceptibility analysis was performed by B.G. and S.B. Ammonite and calcareous nannofossils determinations were performed by I.R. and S.G., respectively. The manuscript was written by G.C. and SB. The manuscript incorporates comments on content and structure from all the authors.

References

Bassoulet, J.P., Elmi, S., Poisson, A., Cecca, F., Bellion, Y., Guiraud, R., & Baudin, F. (1993). Middle Toarcian (184–182 Ma). In: Dercourt, J., Ricou, L.E., Vrielynck, B. (Eds.), Atlas Tethys Paleoenvironmental Maps. Explanatory notes. Gauthiers-Villards, Paris.

Bougeault, C., Pellenard, P., Deconinck, J.-F., Hesselbo, S.P., Dommergues, J.-L., Bruneau, L., Cocquerez, T., Laffont, R., Huret, E., & Thibault, N. (2017). Climatic and palaeoceanographic changes during the Pliensbachian (early Jurassic) inferred from clay mineralogy and stable isotope (C-O) geochemistry (NW Europe). *Global and Planetary Change, 149*, 139–152.

Boulila, S. (2019). Coupling between Grand cycles and Events in Earth's climate during the past 115 million years. *Scientific Reports*. DOI:10.1038/s41598-018-36509-7.

Boulila, S., Brange, C., Cruz, A.M., Laskar, J., Gorini, C., Reis, T.D., & Silva, C.G. (2020). Astronomical pacing of Late Cretaceous third- and second-order sea-level sequences in the Foz do Amazonas Basin. *Marine and Petroleum Geology, 117*, 104382

Boulila, S., Galbrun, B., Hinnov, L.A., & Collin, P.Y. (2008). High-resolution cyclostratigraphic analysis from magnetic susceptibility in a Lower Kimmeridgian (Upper Jurassic) marl-limestone succession (La Méouge, Vocontian Basin, France). *Sedimentary Geology, 203*, 54–63.

Boulila, S., Galbrun, B., Hinnov, L.A., Collin, P.Y., Ogg, J.G., Fortwengler, D., & Marchand, D. (2010). Milankovitch and sub-Milankovitch forcing of the Oxfordian (Late Jurassic) Terres Noires Formation (SE France) and global implications. *Basin Research, 22*, 717-732.

Boulila, S., Galbrun, B., Huret, E., Hinnov, L.A., Rouget, I., Gardin, S., & Bartolini, A. (2014). Astronomical calibration of the Toarcian Stage: Implications for sequence stratigraphy and duration of the early Toarcian OAE. *Earth and Planetary Science Letters, 386*, 98-111.

Boulila, S., Galbrun, B., Laskar, J., & Pälike, H. (2012). A ~9 Myr cycle in Cenozoic $\delta^{13}C$ record and long-term orbital eccentricity modulation. Is there a link? *Earth and Planetary Science Letters, 317–318*, 273–281.

Boulila, S., Galbrun, B., Miller, K.G., Pekar, S.F., Browning, J.V., Laskar, J., & Wright, J.D. (2011). On the origin of Cenozoic and Mesozoic "third-order" eustatic sequences. *Earth-Science Reviews, 109*, 94–112.

Boulila, S., & Hinnov, L.A. (2017). A review of tempo and scale of the early Jurassic Toarcian OAE: Implications for carbon cycle and sea-level variations. *Newsletters on Stratigraphy, 50*, 363-389.

Boulila, S., Laskar, J., Haq, B.U., Galbrun, B., & Hara, N. (2018). Long-term cyclicities in Phanerozoic sea-level sedimentary record and their potential drivers. *Global and Planetary Change, 165*, 128–136.

Bown, P.R., & Cooper, M.K.E. (1988). A calcareous nannofossils biozonation scheme for the early to mid Mesozoic. *Newsletters on Stratigraphy, 20*, 91-114.

Bown, P.R., & Cooper, M.K.E. (1998). Jurassic. In: Bown, P.R. (Ed.), Calcareous Nannofossil Biostratigraphy. Chapman & Hall/Kluwer, Dordrecht, Netherlands, pp. 34–85.

Deconinck, J.F., Hesselbo, S.P., & Pellenard, P. (2019). Climatic and sea-level control of Jurassic (Pliensbachian) clay mineral sedimentation in the Cardigan Bay Basin, Llanbedr (Mochras farm) borehole, Wales. *Sedimentology, 66*, 2769-2783.

de Graciansky, P.C., Jacquin, T., & Hesselbo, S.P. (1998). The Ligurian cycle: an overview of Lower Jurassic 2nd-order transgressive/regressive facies cycles in Western Europe. In: de Graciansky, P.C., Hardenbol, J., Jacquin, T., Vail, P.R. (Eds.), Mesozoic and Cenozoic Sequence Stratigraphy of European Basins. In: *Spec. Publ. - Soc. Econ. Paleontol. Mineral., 60*, 467–479.

Ferreira, J., Mattioli, E., Sucheras-Marx, B., Giraud, F., Duarte, L.V., Pittet, B., Suan, G., Hassler, A., & Spangenberg, J.E. (2019). Western Tethys Early and Middle Jurassic calcareous nannofossils biostratigraphy. *Earth-Science Reviews, 197*, 102908.

Fraguas, A., Comas-Rengifo, M.J., & Perilli, N. (2015). Calcareous nannofossil biostratigraphy of the lower Jurassic in the Cantabrian Range (Northern Spain). *Newsletter on Stratigraphy, 48,* 179-199.

Galeotti, S., Krishnan, S., Pagani, M., Lanci, L., Gaudio, A., Zachos, J.C., Monechi, S., Morelli, G., & Lourens, L. (2010). Orbital chronology of Early Eocene hyperthermals from the Contessa Road section, central Italy. *Earth and Planetary Science Letters, 190*, 192–200.

Gély, J.-P., & Lorenz, J., (1991). Analyse séquentielle du Jurassique (Hettangien á Callovien) du sondage de Couy (Bassin Parisien). *Comptes Rendus de l'Académie des Sciences Paris, 313*, 347–353.

Gély J.P., Lorenz C., Lorenz J., 1996. Les terrains jurassiques du sondage de Couy (Cher, France). Leur analyse séquentielle détaillée à partir de la description des carottes et des courbes diagraphiques. Rev. Inst. Fr. Pét., 51, 3, 319-331.

Ghil, M., Allen, R.M., Dettinger, M.D., Ide, K., Kondrashov, D., Mann, M.E., Robertson, A., Saunders, A., Tian, Y., Varadi, F., & Yiou, P. (2002). Advanced spectral methods for climatic time series. *Review Geophysics, 40*, 1.1–1.41.

Gradstein, F.M., Ogg, J.G., Schmitz, M.D., & Ogg, G.M. (2020). The Geologic Time Scale 2020, 2 volumes, 1390 pp. doi.org/10.1016/C2020-1-02369-3.

Grippo, A., Fischer, A., Hinnov, L., Herbert, T., & Premoli Silva, I., (2004). Cyclostratigraphy and chronology of the Albian stage (Piobbico core, Italy). *Cyclostratigraphy: approaches and Case Histories, 81*, 57-81.

Guillocheau, F. (1991). Mise en évidence de grands cycles transgression-régression d'origine tectonique dans les sédiments mésozoïques du Bassin de Paris. *Comptes Rendus. Academic Science Paris, 312*, 1587–1593.

Guillocheau, F., Robin, C., Allemand, P., Bourquin, S., Brault, N., Dromart, G., Friedenberg, R., Garcia, J.-P., Gaulier, J.-M., Gaumet, F., Grosdoy, B., Manot, F., Le Strat, P., Mettraux, M., Nalpas, T., Prijac, P., Rigollet, C., Serrano, O., & Grandjean, G. (2000). Meso-cenozoic geodynamic evolution of the Paris Basin: 3D stratigraphic constraints. *Geodinamica Acta, 13*, 189–246.

Haq, B.U. (2018). Jurassic sea-level variations: a reappraisal. *GSA Today (Geol. Soc. Am.), 28,* 4–10.

Haq, B.U., Hardenbol, J., & Vail, P.R. (1987). Chronology of fluctuating sea levels since the Triassic. *Science, 235*, 1156–1167.

Haq, B.U., Hardenbol, J., & Vail, P.R. (1988). Mesozoic and Cenozoic chronostratigraphy and cycles of sea-level change. *SEPM, 42*, 71–108.

Hardenbol, J., Thierry, J., Farley, M.B., Jacquin, T., de Graciansky, P.C., & Vail, P.R. (1998). Mesozoic and Cenozoic sequence chronostratigraphic framework of European basins. In: de Graciansky, Hardenbol, P.C.J.., Jacquin, T., Vail, P.R. (Eds.), Mesozoic and Cenozoic Sequence Stratigraphy of European Basins. *Society for Sedimentary Geology (SEPM) Special Publication, 60*, 3–13.

Hays, J.D., Imbrie, J., & Shackleton, N.J. (1976). Variations in the Earth's orbit: Pacemaker of the Ice Ages. *Science, 194*, 1121-1132.

Herbert, T.D. (1999). Toward a composite orbital chronology for the Late Cretaceous and early Paleocene GPTS. *Philosophical Transactions of the Royal Society a-Mathematical Physical and Engineering Sciences, 357*, 1891-1905.

Hermoso, M., Le Callonnec, L., Minoletti, F., Renard, M., & Hesselbo, S.P. (2009). Expression of the Early Toarcian carbon-isotope negative excursion in separated microfractions (Jurassic, Paris Basin). *Earth and Planetary Science Letters, 277*, 194–203.

Hermoso, M., Minoletti, F., Rickaby, R.E.M., Hesselbo, S.P., Baudin, F., & Jenkyns, H.C. (2012). Dynamics of a stepped carbon-isotope excursion: Ultra high-resolution study of Early Toarcian environmental change. *Earth and Planetary Science Letters, 319-320*, 45-54.

Hesselbo SP. (2008). Sequence stratigraphy and inferred relative sea-level change from the onshore British Jurassic. *Proceedings of the Geologists' Association* 119, 19-34.

Hinnov, L.A. (2013). Cyclostratigraphy and its revolutionizing applications in the earth and planetary sciences. *GSA Bulletin, 125 (11/12),* 1703–1734.

Hoang, N.H. Mogavero, F., & Laskar, J. (2021). Chaotic diffusion of the fundamental frequencies in the Solar System. *Astyron. Astrophys. 654*, A156.

Huang, Z., Boyd, R., & O'Connel, S. (1992). Upper cretaceous cyclic sediments from hole 762C, exmouth plateau, northwest Australia. In: In: Van Rad, U., Haq, B.U. (Eds.), Proc. Ocean Drilling Program, vol. 122. *Scientific Response* 259–277.

Huang, C., Hesselbo, S., & Hinnov, L. (2010a). Astrochronology of the late Jurassic Kimmeridge Clay (Dorset, England) and implications for Earth system processes. *Earth and Planetary Science Letters, 289*, 242-255.

Huang, C., Hinnov, L., Fisher, A.G., Grippo, A., & Herbert, T. (2010b). Astronomical tuning of the Aptian Stage from Italian reference sections. *Geology, 38*, 899-902.

Ikeda, M., & Tada, R. (2014). A 70 million year astronomical time scale for the deep-sea bedded chert sequence (Inuyama Japan): Implications for Triassic-Jurassic geochronology. *Earth and Planetary Science Letters, 399*, 30-43.

Ikeda, M., Tada, R., & Sakuma, H. (2010). Astronomical cycle origin of bedded chert: A middle Triassic bedded chert sequence, Inuyama, Japan. *Earth and Planetary Science Letters, 297*, 369-378.

Jacquin, T., Dardeau, G., Durlet, C., de Graciansky, P.C., & Hantzpergue, P. (1998). The North Sea cycle: An overview of 2nd order transgressive/regressive facies cycles in Western Europe. *SEPM Special Publication, 60*, 445–446.

Kodama, K. P., & Hinnov, L. A. (2014). Rock Magnetic Cyclostratigraphy, New Analytical Methods in Earth and Environmental Science Series, Wiley-Blackwell.

Laskar, J. (1989). A numerical experiment on the chaotic behaviour of the Solar System. *Nature, 338,* 237–238.

Laskar, J. (1990). The chaotic motion of the Solar System: a numerical estimate of the size of the chaotic zones. *Icarus, 88*, 266–291.

Laskar, J. (2020). Astrochronology, in Geologic Time Scale 2020, Gradstein et al, eds, Elsevier.

Laskar, J., Fienga, A., Gastineau, M., & Manche, H. (2011). La2010: a new orbital solution for the long-term motion of the Earth. *Astron. Astrophys. 532*, A89. Doi:10.1051/0004-6361/201116836.

Laskar, J., Robutel, P., Joutel, F., Gastineau, M., Correia, A.C.M., & Levrard, B. (2004). A long-term numerical solution for the insolution quantities of the Earth. *Astron. Astrophys., 428*, 261–285.

Li, M., Kump, L.R., Hinnov, L.A., & Mann, M.E. (2018). Tracking variable sedimentation rates and astronomical forcing in Phanerozoic paleoclimate proxy series with evolutionary correlation coefficients and hypothesis testing. *Earth Planetary Science Letters, 501*, 165-179.

Lithwick, Y., & Wu, Y. (2011). Theory of secular chaos and Mercury's orbit. *Astrophys. J., 739*, 31.1–17.

Lorenz, J., Lefavrais, A., Depeche, F., Leclerc, V., Marchand, D., Roy, B., Taugourdeau, J., & Reyre, Y. (1987). Le Jurassique. In: Lorenz, C. (Ed.), Forage scientifique de Sancerre-Couy (Cher). In: Documents du Bureau de Recherches Géologiques et Minières, vol. 136. Bureau de Recherches Géologiques et Minières, pp. 19–26.

Lorenz, C., Lefavrais, A., Lorenz, J., Marchand, D., & Million, R. (1991). Calage stratigraphique des diagraphies du Jurassique du sud du bassin Parisien à partir du sondage de Sancerre–Couy (Programme Géologie profonde de la France). *Bulletin de la Société Géologique de France, 162*, 947–952.

Ma, C., Meyers, S. R., & Sageman, B. B. (2017). Theory of chaotic orbital variations confirmed by Cretaceous geological evidence. *Nature, 542*, 468–470.

Ma, C., Meyers, S.R., & Sageman, B.B. (2019). Testing Late Cretaceous astronomical solutions in a 15 million year astrochronologic record from North America. *Earth and Planetary Science Letters, 513*, 1-11.

Martinez, M., & Dera G. (2015). Orbital pacing of carbon fluxes by a 9 My eccentricity cycle during the Mesozoic, *PNAS, 112*, 12604-12609.

Mattioli, E., & Erba E. (1999). Biostratigraphic synthesis of calcareous nannofossil events in the Tethyan Jurassic, Rivista Ital. *Paleontol. Stratigr., 105*, 343–376.

Mau, M., Kent, D.V., & Clemmensen, L.B. (2022). Planetary chaos and inverted climate phasing in the late Triassic of Greenland. *PNAS 119*, 1-7.

Mayer, H., & Appel, E. (1999). Milankovitch cyclicity and rock-magnetic signatures of paleoclimatic changes in the early cretaceous biancone formation of the southern alps. Italy. *Cretaceous Research, 20*, 189–214.

McArthur, J.M., Donovan, D.T., Thirlwall, M.F., Fouke, B.W., & Mattey, D. (2000). Strontium isotope profile of the early Toarcian (Jurassic) oceanic anoxic event, the du- ration of ammonite biozones, and belemnite palaeotemperatures. *Earth Planetary Science Letters, 179*, 269–285.

Meyers, S. R., & Sageman, B. B. (2007). Quantification of deep-time orbital forcing by average spectral misfit. *American Journal of Science, 307*, 773–792. doi: 10.2475/05. 2007.01

Meyers, S.R., Sageman, B.B., & Hinnov, L.A. (2001). Integrated quantative stratigraphy of the Cenomanian-Turonian Bridge Creek Limestone Member using evolutive harmonic analysis and stratigraphic modeling. *Journal of Sedimentary Research* 71, 628–644.

Milankovitch, M. (1941). Kanon der Erdbestrahlung und seine Anwendung auf das Eiszeitenproblem. *Spec. Acad. R. Serbe*, Belgrade.

Mogavero, F., & Laskar, J. (2022). The origin of chaos in the Solar System through computer algebra. *Astron. Astrophys. Letters*, in press, DOI: https://doi.org/10.1051/0004-6361/202243327.

Muller, R.A., & MacDonald, G.J. (2000). Ice Ages and Astronomical Causes: Data, Spectral Analy-sis and Mechanisms. *Chichester, UK, Praxis Pub-lishing*, 318 p.

Olsen, P.E. & Kent, D.V. (1999). Long-period Milankovitch cycles from the Late Triassic and Early Jurassic of eastern North America and their implications for the calibration of the Early Mesozoic time–scale and the long–term behaviour of the planets. *Philosophical Transactions of the Royal Society of London, 357*, 1761-1786.

Olsen, P.E., Laskar, J., Kent, D.V., Kinney, S.T., Reynolds, D.J., Sha, J., & Whiteside, J.H. (2019). Mapping Solar System chaos with the Geological Orrery *PNAS, 116,* 10664-10673 doi/10.1073/pnas.1813901116.

Paillard, D., Labeyrie, L., & Yiou, P. (1996). Macintosch program performs timeseries analysis. *Eos, 77,* 379.

Pälike, H., Norris, R.D., Herrle, J.O., Wilson, P.A., Coxall, H.K., Lear, C.H., Shackleton, N.J., Tripati, A.K., & Wade, B.S. (2006). The heartbeat of the oligocene climate system. *Science, 314*, 1894–1898.

Peti, L., Thibault, N., Clémence, M.-E., Korte, C., Dommergues, J.-L., Bougeault, C., Pellenard, P., Jelby, M.E., & Ullmann, C.V. (2017). Sinemurian–Pliensbachian calcareous nannofossil biostratigraphy and organic carbon isotope stratigraphy in the Paris Basin: Calibration to the ammonite biozonation of NW Europe. *Palaeogeography, Palaeoclimatology, Palaeoecology, 468*, 142-161.

Peti, L., Thibault, N., Korte, C., Ullmann, C.V., Cachao, M., & Fibaek, M. (2021). Environmental drivers of size changes in lower Jurassic Schizosphaerella spp. *Marine Micropaleontology in press*, 102053.

Pieńkowski, G., Uchman, A., Ninard, K., & Hesselbo, S.P. (2021). Ichnology, sedimentology, and orbital cycles in the hemipelagic Early Jurassic Laurasian Seaway (Pliensbachian, Cardigan Bay Basin, UK). *Global and Planetary Change, 207,* 103648.

Roth, P.H. (1984). Preservation of calcareous nannofossils and fine-grained carbonate particles in mid-Cretaceous sediments from the southern Angola Basin. In: Hay, W.W., Sibuet, J.C., Barron E.J. et al. (Eds.), Init. Rept. DSDP 75, U.S. Govt. Printing O/ce, Washington, DC, 651–655.

Roth, P.H., & Thierstein, H.R. (1972). In: Hayes, D.E., Pimm, A.C., et al. (Eds.), Calcareous nannoplankton: Leg 14 of the Deep Sea Drilling Project. Initial Rep. DSDP, vol. 14, U.S. Govt. Printing Office, Washington, 421–486.

Ruebsam, W., & Al-Husseini, M. (2021). Orbitally synchronized late Pliensbachian-early Toarcian glacio-eustatic and carbon -isotopes cycles. *Palaeogeography, Palaeoclimatology, Palaeoecology, 577*, 110562.

Ruebsam, W., Mayer, B., & Schwark, L. (2019). Cryosphere carbon dynamics control early Toarcian global warming and sea level evolution. *Global and Planetary Change, 172,* 440-453.

Ruebsam, W., Münzberger, P., & Schwark, L. (2014). Chronology of the Early Toarcian environmental crisis in the Lorraine Sub-Basin (NE Paris Basin). *Earth and Planetary Science Letters, 404,* 273-282.

Ruhl, M., Hesselbo, S.P., Hinnov, L., Jenkyns, H.C., Xu, W., Riding, J.B., Storm, M., Minisini, D., Ullmann, C.V. & Leng, M.J. (2016). Astronomical constraints on the duration of the Early Jurassic Pliensbachian Stage and global climatic fluctuations. *Earth and Planetary Science Letters, 455*, 149-165.

Simmons, M.D. (2012). Sequence stratigraphy and sea level change, *in* F. M. Gradstein, J. G. Ogg, M. Schmitz, and G. Ogg, eds., The geologic time scale 2012, 1st Edition: Amsterdam, Elsevier, v. 1, pp. 239–267.

Simmons, M. D., Sharland, P.R., Casey, D.M., Davies, R.B., & Sutcliffe, O.E. (2007). Arabian Plate sequence stratigraphy: Potential implications for global chronostratigraphy. *GeoArabia, 12,* 101–130.

Simmons, M.D., Miller, K.G., Ray, D.C., Davies, A., van Buchem, F.S.P., & Gréselle, B. (2020). Phanerozoic eustasy. In: Gradstein, F.M., Ogg, J.G., Schmitz, M.D., Ogg, G.M. (Eds.), The Geologic Time Scale 2020. v.1, pp. 357–400.

Sprovieri, M., Sabatino, N., Pelosi, N., Batenburg, S.J., Coccioni, R., Iavarone, M., & Mazzola, S. (2013). Late Cretaceous orbitally-paced carbon isotope stratigraphy from the Bottaccione Gorge (Italy). *Palaeogeography Palaeoclimatology Palaeoecology 379–380*, 81–94.

Storm, M.S., Hesselbo, S.P., Jenkyns, H.C., Ruhl, M., Ullmann, C.V., Xu, W., Leng, M.J., Riding, J.B., & Gorbadenko, O. (2020). Orbital pacing and secular evolution of the Early Jurassic carbon cycle. *PNAS, 117*, 3974-3982. doi/10.1073/pnas.1912094117

Sussman, G. J. & Wisdom, J. (1988). Numerical evidence that the motion of Pluto is chaotic. *Science, 241*, 433-437.

Taner, M.T. (2000). Attributes Revisited, Technical Publication. Rock Solid Images, Inc., Houston, Texas. URL: http://www.rocksolidimages.com/pdf/attrib_revisited.htm.

Thierry, J., et al. (40 co-authors) (2000). Late Sinemurian. *In*: Dercourt, J., Gaetani, M. et al. eds., Atlas Peri-Tethys, *Palaeogeographical maps*. CCGM/ CGMW, Paris, map 7.

Thomson, D.J. (1982). Spectrum estimation and harmonic-analysis. *Proceedings of the IEEE 70*, 1055–1096.

Ullmann, C.V., Szucs, D., Jiang, M., Hudson, A.J.L., & Hesselbo, S.P. (2022). Geochemistry of macrofossil, bulk rock and secondary calcite in the Early Jurassic strata of the Llanbedr (Mochras Farm) drill core, Cardigan Bay Basin, Wales, UK. Journal of the Geological Society 179, doi.org/10.1144/jgs2021-018.

Vail, P.R., Mitchum, R.M., Todd, J.R.G., Widmier, J.M., Thompson, S., Sangree, J.B., Bubb, J.N., & Hatlelid, W.G. (1977). Seismic stratigraphy and global changes of sea level. In: Payton, C.E. (Ed.), Seismic Stratigraphy – Applications to Hydrocarbon Exploration. In: AAPG Mem., vol. 26, pp. 49–212.

Williams, C.J., Hesselbo, S.P., Jenkyns, H.C., & Morgans-Bell, H.S. (2001). Quartz silt in mudrocks as a key to sequence stratigraphy (Kimmeridge Clay Formation, Late Jurassic, Wessex Basin, UK). *Terra Nova 13*, 449-455.

Wolf, A., 1986. Quantifying Chaos With Lyapunov Exponents. In A. Holden Eds. *"Nonlinear science: Theory and Applications"*. Manchester University Press, 1986.

Wu, H., Zhang, S., Hinnov, L.A., Jiang, G., Feng, Q., Li, H., & Yang, T. (2013a). Time-calibrated Milankovitch cycles for the late Permian. *Nature Communications 4*, 2452-2459 doi:10.1038/ncomms3452.

Wu, H., Zhang, S., Jiang, G., Hinnov, L., Yang, T., Li, H., Wan, X., & Wang, C. (2013b). Astrochronology of the Early Turonian-Early Campanian terrestrial succession in the

Songliao Basin, northeastern China and its implications for long-period behavior of the Solar System. *Palaeogeography, Palaeoclimatology, Palaeoecology 385*, 55-70.

Zachos, J. C., Pagani, M., Sloan, L., Thomas, E., & Billups, K. (2001). Trends, Rhythms, Aberrations in Global Climate 65 Ma to Present. *Science 292*, 686–693.

Supplementary information on:

A 20-million-year Early Jurassic cyclostratigraphic record and its implications for the chaotic inner Solar System and sea-level changes

Guillaume Charbonnier[1*], Slah Boulila[1,2], Bruno Galbrun[1], Jacques Laskar[2], Silvia Gardin[3], Isabelle Rouget[3]

1. Time series analysis

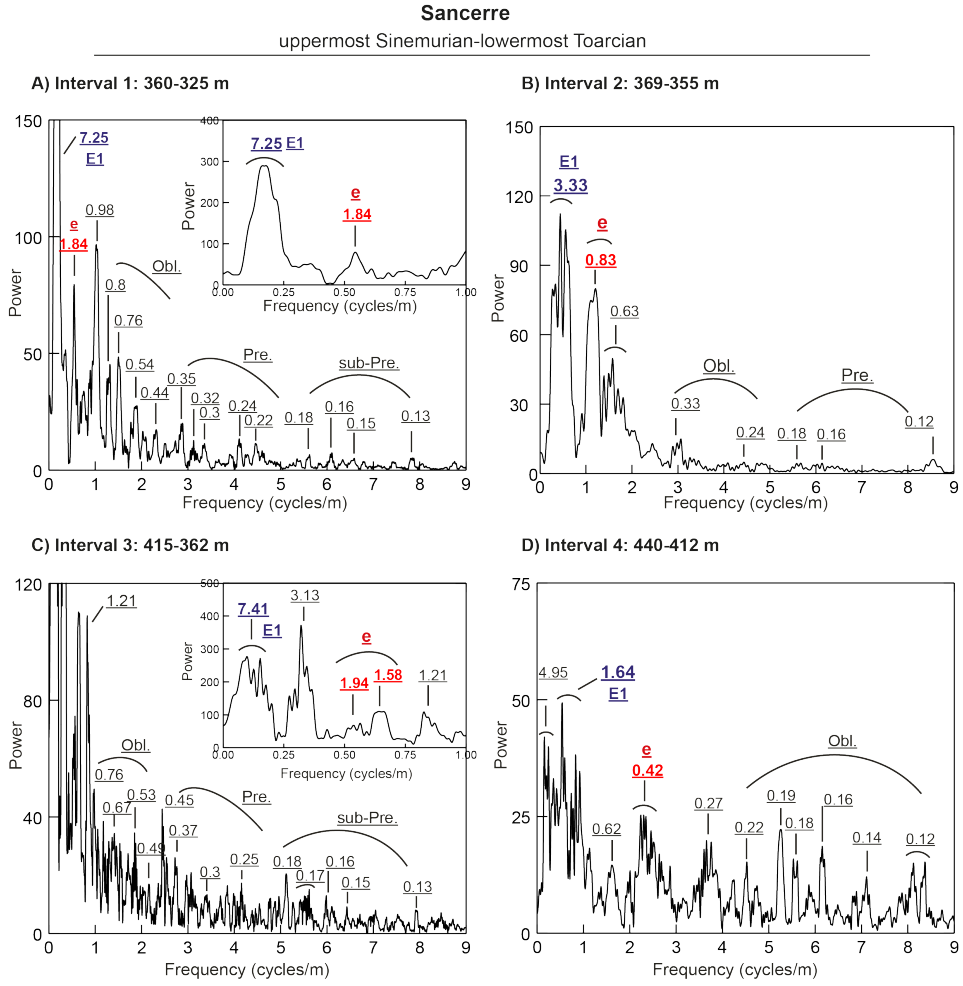

Fig. S1: 2π-MTM power spectra for four intervals (shown in Fig. 4) of the detrended magnetic susceptibility (MS, with a 30% weighted average smoothing) data is obtained using

14 the multitaper method (Thomson, 1982) as implemented in SSA-MTM Toolkit (Ghil et al.,
15 2002). **A)** Untuned interval from 360 to 325 m, with the two high-power peaks in the low
16 frequencies (7.25- and 1.84-m wavelengths) truncated to emphasize the high frequency
17 portion of the spectrum. *Inset:* spectrum over [0, 1 cycles/m]. **B)** Untuned interval from 369 to
18 355 m. **C)** Untuned interval from 415 to 362 m, with the high-power peaks in the low
19 frequencies (7.41-, 3.13-, 1.94-, and 1.58-m wavelengths) truncated to emphasize the high
20 frequency portion of the spectrum. *Inset:* spectrum over [0, 1 cycles/m]. **D)** Untuned interval
21 from 440 to 412 m. Most peaks are labelled in meters.

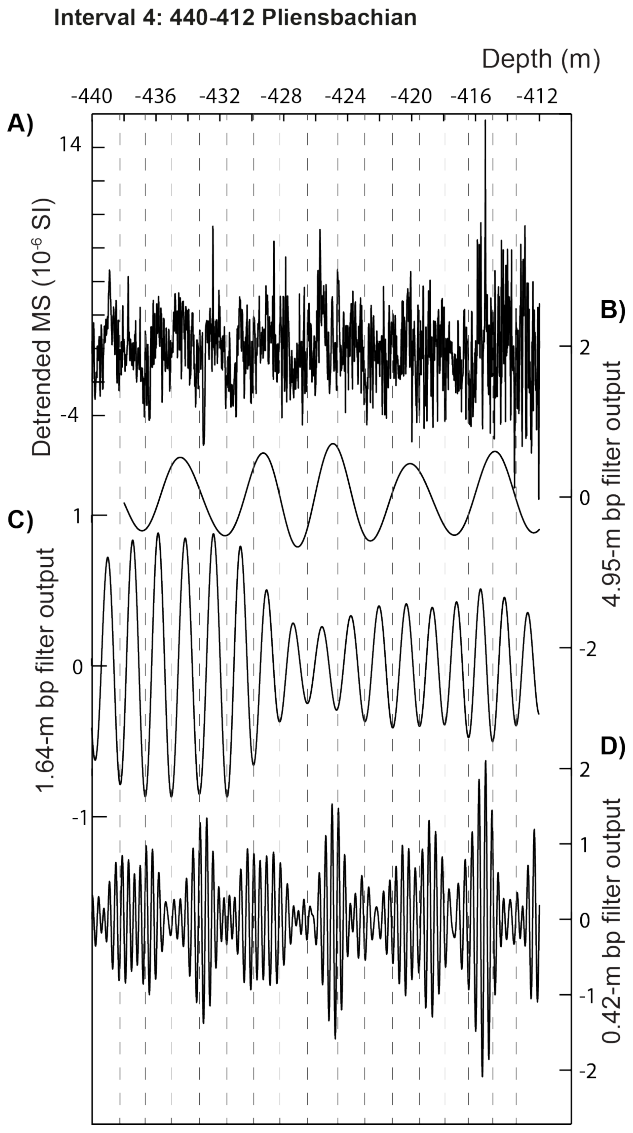

22

23 **Fig. S2:** Detail of the Pliensbachian interval showing the gradual variations of MS values. **(A)**
24 Detrended MS data from 440 to 412 m (Interval 4) with **(B)** cutoff frequencies 0.122 and

0.282 cycles-m to isolate 4.95-m, **(C)** cutoff frequencies 0.56 and 0.66 cycles-m to isolate 1.64-m (405-kyr eccentricity cycle), and **(D)** cutoff frequencies 2.31 and 2.61 cycles-m to isolate 0.42-m (short eccentricity cycle). Spectral analysis of this interval is shown in Fig. 3 (interval 4).

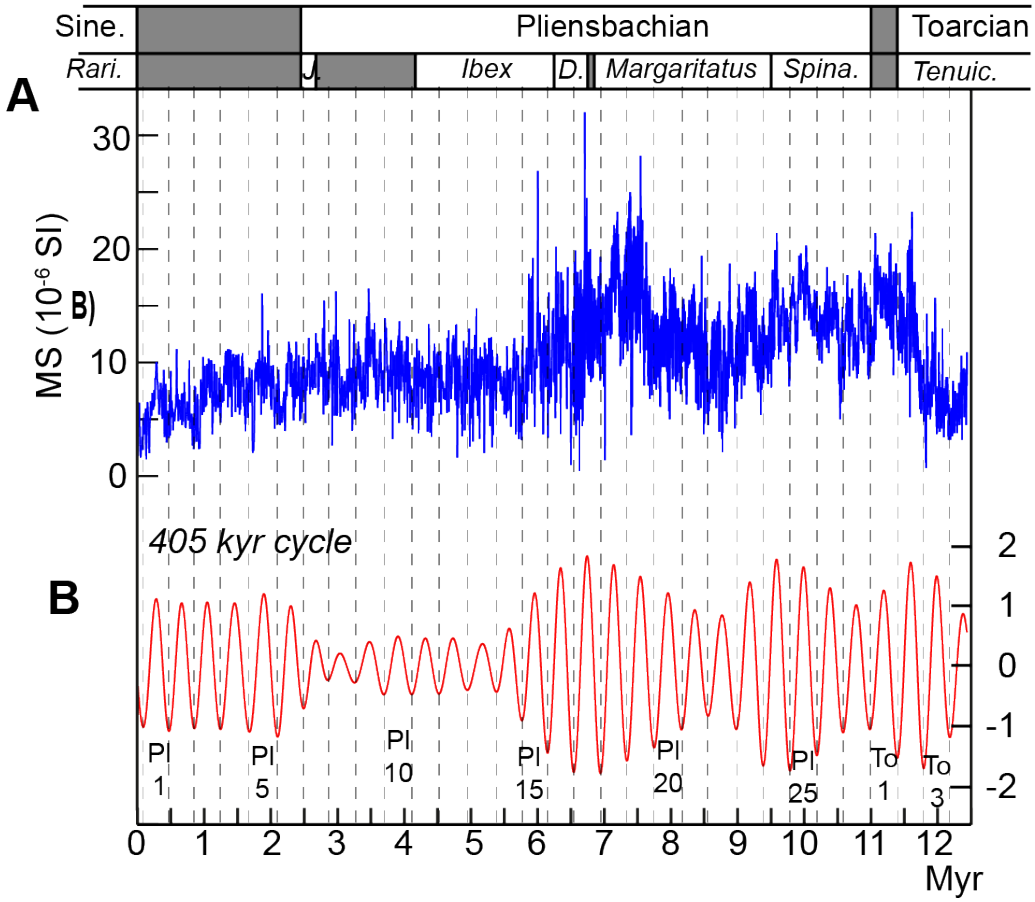

Fig. S3: A) 405-kyr tuned MS series spanning the latest Sinemurian through earliest Toarcian with a 30% weighted average smoothing. **B)** Bandpass filtering of the 405-kyr eccentricity cycle (g2-g5; cutoff frequencies 0.00221 and 0.00271 cycles/kyr). The Pl1 to To3 cycles are the interpreted 405-kyr eccentricity cyclicities.

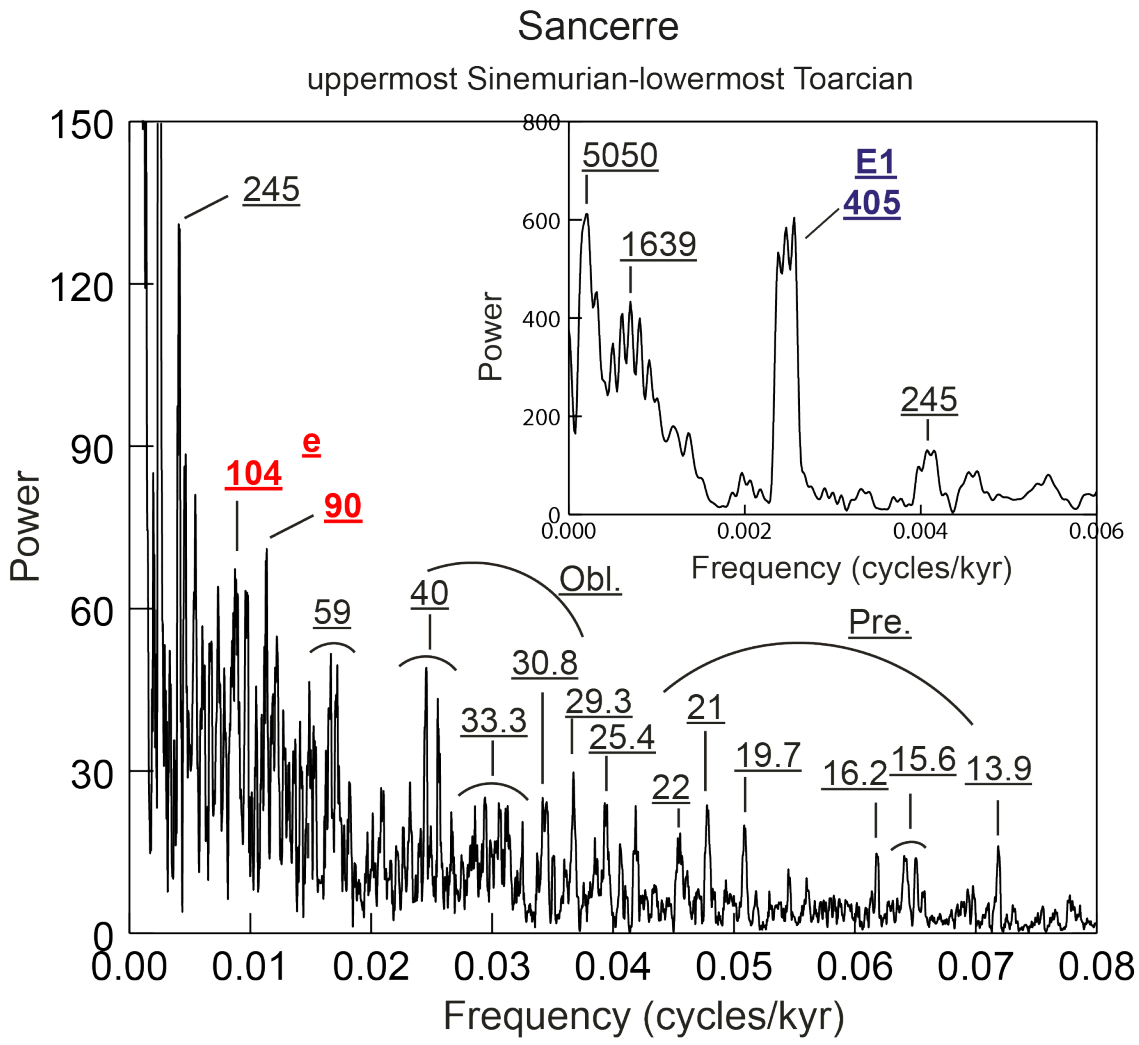

Fig. S4: Spectrum of the detrended 405 kyr tuned MS series (with a 30% weighted average smoothing) for the latest Sinumerian-earliest Turonian interval with the three high-power peaks in the low frequencies (5050, 1639- and 450-kyr periods) truncated to emphasize the high-frequency portion of the spectrum. *Inset*: spectrum over [0, 0.003 cycles/kyr] expands the low-frequency spectrum.

A)

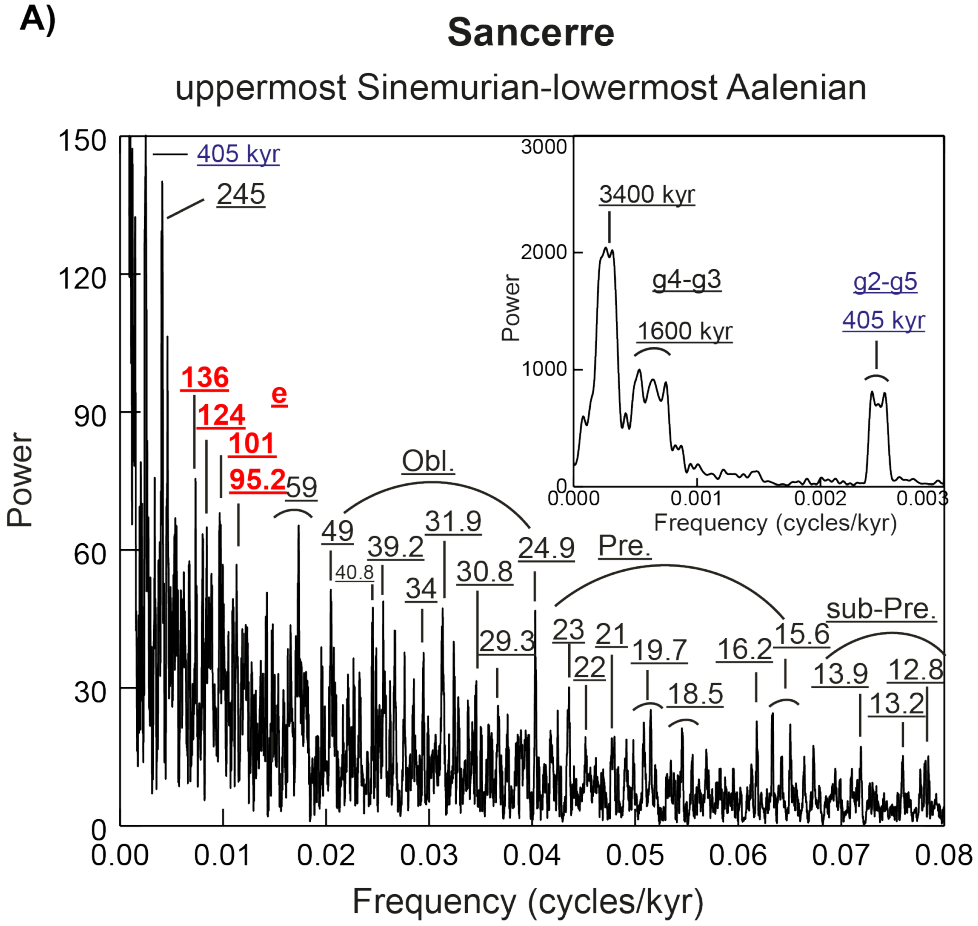

B) **Spectrum of La20004 astronomical parameters**

193.9-173.9 Ma

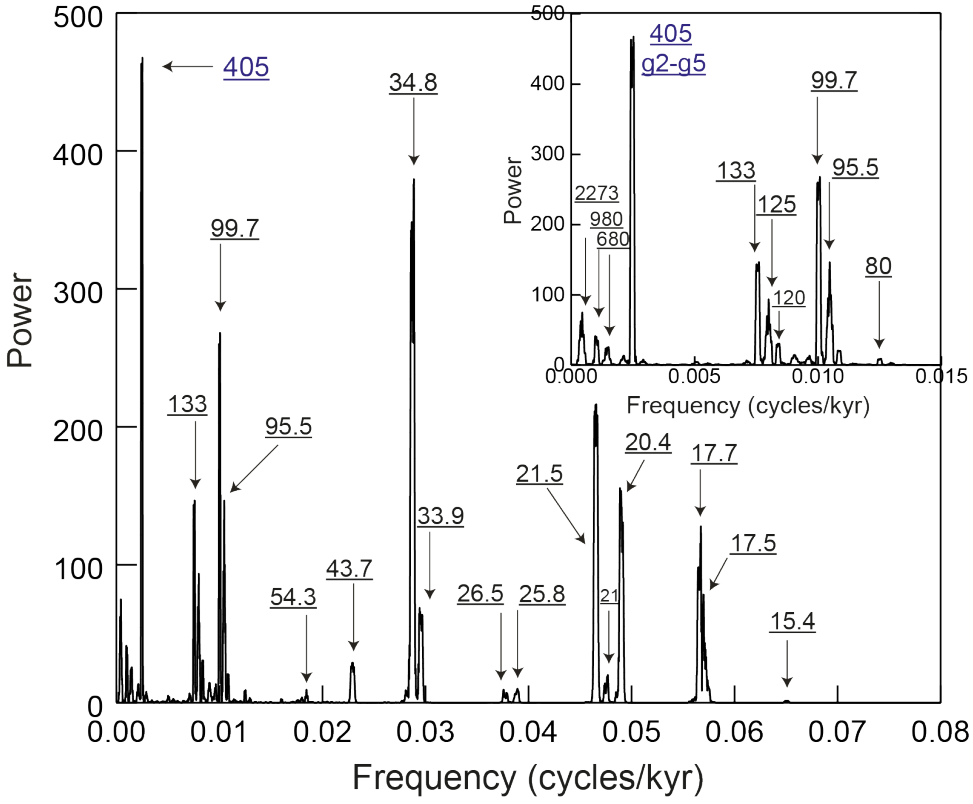

Fig. S5: (A) Spectrum of the detrended 405 kyr tuned MS series (with a 30% weighted average smoothing) for the latest Sinemurian-earliest Aalenian interval with the three high-power peaks in the low frequencies (3600, 1600- and 450-kyr periods) truncated to emphasize the high-frequency portion of the spectrum. *Inset*: spectrum over [0, 0.003 cycles/kyr] expands the low-frequency spectrum. **(B)** Spectrum of La2004 astronomical parameters (Laskar et al., 2004) in ETP format (Eccentricity, Tilt, Precession) for the interval 193.9-173.9 Ma, corresponding to the uppermost Sinemurian-lowermost Aalenian interval according to GTS2020 (Gradstein et al., 2020). *Inset*: amplitude spectrum over [0, 0.015 cycles/kyr] details periodic compounds of the low-frequency spectrum. Peaks are labelled in kyr.